A bounding surface model for cemented soil at small and large strains

Authors: Kang-fu Jiao[1]; and Chao Zhou*[2]

*Corresponding author

Information of the authors

[1] Ph.D. Student, Department of Civil and Environmental Engineering, The Hong Kong Polytechnic University, Hung Hom, Kowloon, Hong Kong.

Email: kangfu.jiao@connect.polyu.hk

[2] Tsui Tack Kong Young Scholar in Civil Engineering, Associate Professor, Department of Civil and Environmental Engineering, The Hong Kong Polytechnic University, Hung Hom, Hong Kong; The Hongkong Polytechnic University Shenzhen Research Institute.

Email: c.zhou@polyu.edu.hk

Abstract

Many constitutive models have been proposed to describe the mechanical behaviour of cemented soil at large strains (above 1%). Less attention has been paid to the highly non-linear stress-strain behaviour at small strains, which are important for accurately analysing the serviceability of many infrastructures. In this study, a bounding surface model was developed to simulate cemented soil behaviour from small to large strains. Some new formulations were proposed to improve the modelling of small-strain behaviour, including (i) the elastic shear modulus over a wide range of stress conditions; (ii) the non-linear degradation of bonding strength (p_b) with damage strain (ε_d) in the $ln\, p_b - \varepsilon_d$ plane. The new model was applied to simulate drained and undrained triaxial tests on cemented soils at different cement contents and confining pressures. Comparisons between the measured and computed results show that the new model can well capture many important aspects of cemented soil behaviour, especially the elastic shear modulus at very small strains and stiffness degradation at small strains. Furthermore, the model gives a good simulation of strain softening/hardening and dilatancy/contraction during shearing under various confining pressure and void ratio conditions.

Keywords: constitutive model, bounding surface plasticity, cemented soil, small strains

Introduction

Ground improvement with cement has been widely used in engineering practice (Acar and Eltahir, 1986; Watabe and Noguchi, 2011; Ni et al., 2016; Yamada et al., 2022). So far, extensive experimental studies have been conducted to investigate the mechanical behaviour (Marri et al., 2012; Xiao et al., 2014) and microstructure (Clough et al., 1981; Kamruzzaman et al., 2009; Nguyen et al., 2017) of cemented soil. The experimental results generally show that the presence of cementation bonds can increase soil stiffness (Nguyen et al., 2017), peak and critical state strength (Clough et al., 1981) and dilatancy (Consoli et al., 2000; Wang and Leung, 2008). The cementation bonds break under external loading, leading to a more pronounced strain-softening behaviour (Sasanian, 2011). Furthermore, similar to uncemented soil, the stress-strain behaviour of cemented soil is highly non-linear. With an increase in strain from 0 to 1%, soil stiffness may decay by orders of magnitude (Atkinson, 2000). According to field data in the literature (Melentijevic et al., 2013; Voottipruex et al., 2019; Pongsivasathit et al., 2021), typical soil strains encountered in cement-improved engineering structures, such as embankments stabilised by deep cement mixing piles, mainly fall in the small strain range. An accurate prediction of cemented soil behaviour in a small strain range is thus essential for predicting the performance of infrastructures at their working conditions.

Many constitutive models have been developed for cemented soil based on valuable experimental results. A common feature of these models is incorporating a cementation strength parameter that increases with cement content and decreases with plastic strain. Such a parameter is used to modify different components of a constitutive model, particularly the yield surface. Most of the existing constitutive models were proposed within the classical elastoplastic framework (e.g., Hirai et al., 1989; Namikawa and Mihira, 2007; Nguyen et al., 2014; Horpibulsuk et al., 2010) with a focus on the strain-softening and dilative behaviour of cemented soil. These models cannot well capture the non-linear stress-strain behaviour and

stiffness degradation in the small strain range since only elastic deformation is predicted when the stress state is inside the yield surface. Several advanced models have recently been developed based on the bounding surface theory (Ravanbakhsh and Hamidi, 2013; Xiao et al., 2017; Zhang et al., 2023). These models improve the prediction of gradual yielding and soil behaviour under cyclic loading. However, the development of these bounding surface models did not pay particular attention to the mechanical behaviour of cemented soil at small strains. They may not be able to simulate the small strain stiffness of cemented soil very well for several reasons:

(i) There are two common methods of modelling the elastic shear modulus G_0, often corresponding to the very small strain range (below 0.001%). Some models calculate G_0 from the swelling index and Poisson's ratio, like Nguyen et al. (2017). This method is simple but cannot accurately calculate G_0. In other models, like Trhlíková et al. (2012) and Zhang et al. (2023), G_0 is calculated by semi-empirical equations incorporating the effects of void ratio, effective stress and cementation. The existing semi-empirical equations do not work well when the stress is relatively low (e.g., predicting a negative shear modulus at tensile stress conditions), as discussed later in detail.

(ii) The degradation of cementation bonds is crucial for predicting the behaviour of cemented soil at any strain level. The commonly-used formulas often overestimate the bond degradation and thus underestimate soil stiffness in the small strain range. More discussion is given in the section on mathematical formulations.

This study developed a new state-dependent critical state model to capture the behaviour of cemented soil at small and large strains. As far as the authors are aware, this is the first model for the small-strain behaviour of cemented soil, i.e., the degradation of shear modulus with strain at small strains (<1%). The model is based on the bounding surface plasticity theory (Dafalias, 1986). To capture the degradation of the modulus in the small strain range, a new

formula for calculating the shear modulus and a new formula for describing the cementation degradation is proposed. Previously published results of triaxial drained and undrained tests on various cemented soils were used to verify the new model. In this paper, model formulations and parameter calibration are described in detail.

Mathematical formulations

The proposed model is formulated in the triaxial stress space. The soil stress state is defined using the effective mean stress (p') and deviator stress (q). The deformation is described through the volumetric strain (ε_v) and deviator strain (ε_q). For sign convention, compressive stress and strain are considered positive.

Elastoplasticity

Following the bounding surface plasticity theory proposed by Dafalias (1986), the total strain consists of elastic and plastic parts:

$$\begin{cases} d\varepsilon_v = d\varepsilon_v^e + d\varepsilon_v^p \\ d\varepsilon_q = d\varepsilon_q^e + d\varepsilon_q^p \end{cases} \tag{1}$$

where $d\varepsilon_v$, $d\varepsilon_v^e$ and $d\varepsilon_v^p$ are the total, elastic and plastic increments of the volumetric strain, respectively; and $d\varepsilon_q$, $d\varepsilon_q^e$ and $d\varepsilon_q^p$ are the total, elastic and plastic increments of the deviator strains, respectively. The incremental elastic strains are calculated using the following formulation:

$$\begin{cases} d\varepsilon_q^e = \frac{dq}{3G_0} \\ d\varepsilon_v^e = \frac{dp'}{K} \end{cases} \tag{2}$$

where K is the bulk modulus and G is the shear modulus. The incremental plastic strains are expressed as follows:

$$\begin{cases} d\varepsilon_v^p = D\Lambda \\ d\varepsilon_q^p = \Lambda \end{cases} \tag{3}$$

where $D = d\varepsilon_v^p / d\varepsilon_q^p$ is the dilatancy index; and Λ is the non-negative loading index. The

dilatancy and loading index can be obtained from the flow rule and the hardening law, which are explained later.

Bounding and yield surfaces

As summarised and illustrated by Dafalias (1986), the main feature of bounding surface models is the dependency of the plastic modulus on the distance between actual and 'imaged' stress states. In addition to this general feature, each bounding surface model has some specific features regarding the definition and description of the bounding surface (Zhou et al., 2015). The current model adopts the approach of Wang et al. (1990). Two bounding surfaces are defined in the p'-q plane, as shown in Figure 1, both of which intersect with the horizontal axis at the point (p_b, 0). The variable p_b is defined as cementation bond strength and used to describe cementation effects on soil strength. Its initial value and loading-induced evolution are discussed in the next section.

The first bounding surface is the maximum prestress memory bounding surface. It can be described as follows:

$$F_s = q - M_m(p' + p_b) \tag{4}$$

where M_m is the maximum value of stress ratio $q/(p' + p_b)$ in the stress history.

The other one is the failure bounding surface, which is mathematically defined as follows:

$$\overline{F_s} = q - M_b(p' + p_b) \tag{5}$$

$$M_b = M_c exp(-n_b \Psi) \tag{6}$$

where M_c is the critical state stress ratio; M_b is the attainable peak stress ratio; and n_b is a positive model parameter used to define the influence of the state parameter on the strength. The location of the failure bounding surface depends on the state variable Ψ, which is defined later. According to equation (6), when Ψ is positive and negative, M_b is below and above M_c, respectively.

Furthermore, a yield surface is defined in the p'-q plane using equation (7) representing

the elastic range under shearing (Zhou et al., 2015). Within this elastic range, soil deformation is considered elastic.

$$f_t = \left|\frac{q}{p'+p_b} - \alpha\right| - m_c \tag{7}$$

where p_b is the cementation bond strength, as defined above, and its determination is given in the next section. m_c is a model parameter governing the size of the elastic region (see Figure 1). Following some previous studies (Dafalias and Manzari, 2004; Zhou et al., 2020), a default and constant value of 0.01 is used for this parameter. This simplification barely affects the model prediction because the elastic range of soils with constant stiffness is usually very small (in the order of 0.001%). On the other hand, the variable α corresponds to the back stress ratio (Dafalias and Manzari, 2004), which depends on the stress path. When the stress state is on the yield surface, and the soil is subjected to continuous shearing, soil behaviour is elastoplastic and α changes to ensure that the stress state remains on the yield surface. For other cases, soil behaviour is elastic, and α maintains constant. The determination and evolution of α were described by Zhou et al. (2020) in detail.

The current model does not define bounding and yield surfaces for compression, assuming that soil behaviour under loading and unloading at a constant stress ratio is elastic. In this way, only the changes in stress ratio ($q/(p'+p_b)$) can cause significant particle rearrangements, which are macroscopically modelled as plastic shear and volume changes (Dafalias and Manzari, 2004; Taiebat and Dafalias, 2008). For most practical purposes, the plastic strain due to a stress increase under a constant stress ratio can be neglected (Wang and Xie, 2014), especially for cemented soils with a high yield stress during constant stress ratio compression. It is worth mentioning that this simplification has been widely adopted in previous research (Manzari and Dafalias, 1997; Dafalias and Manzari, 2004; Wang and Xie, 2014; Doherty and Wood, 2020; Zhang et al., 2023). This method can keep the model relatively simple and reduce at least two model parameters related to the hardening and dilatancy during constant stress ratio

compression (Zhou and Ng, 2016).

Cementation bond strength

The cement hydration and pozzolanic reactions produce cementation bonds between soil particles, which can significantly improve soil strength and stiffness (Clough et al., 1981; Doherty and Wood, 2020). The unconfined compression strength of cemented soil is usually considered a power function of cement content (Consoli et al. 2007). Similarly, the relationship between initial cementation bond strength p_{b0} and cement content is modelled using a power function:

$$p_{b0} = k_{pb} Cc^{\beta} \tag{8}$$

where Cc is the cement content; the constant of proportion k_{pb} is a soil parameter used to determine the magnitude of the bond strength at different cement contents; the power β is a soil parameter that characterizes the sensitivity of bond strength to cement content. The parameters k_{pb} and β characterize the initial bond strength of a specimen following the curing process but before any mechanical loading. Various factors, including soil properties, binder type, curing condition and duration, influence the value of these two parameters. For simplicity, the values of k_{pb} and β are determined for each specific material, curing condition and duration. Once the curing is complete, these parameter values remain constant during subsequent compression and shearing. For example, some experimental investigations have shown that the presence of curing stress (i.e. confinement during the cement hydration reaction) will lead to a significant increase in bond strength (Cuccovillo and Coop, 1999; Fernandez and Santamarina, 2001; Vatsala et al., 2001; Yun and Santamarina, 2005; Nweke, 2017). This influence on initial bond strength is considered by changing the value of k_{pb} and β in the proposed model. On the other hand, changing confinement after curing can lead to cementation degradation, which is explained below.

An accurate prediction of cementation bond strength degradation is very important for

predicting the mechanical behaviour of cemented soil. Suebsuk et al. (2010) and Zhang et al. (2023) related the debonding process to plastic deviator strain for simplicity, and this cannot reflect the debonding induced by plastic volumetric strain. In the current model, the cementation bond strength p_b is modelled as a function of damage strain following the approach of Baudet and Stallebrass (2004):

$$\varepsilon_d = \sqrt{\varepsilon_q^{p\,2} + \varepsilon_v^{p\,2}} \tag{9}$$

$$p_b = p_{b0}\exp\left(-\left(\frac{\varepsilon_d}{\varepsilon_{ref}}\right)^k\right) \tag{10}$$

where ε_d is the damage strain; k and ε_{ref} are two parameters used to describe the rate of p_b degradation. It is important to acknowledge that various functions could be employed to model the bonding strength degradation, even though they may not be equally efficient. Equation (10) adopts an exponential function because it is found able to effectively capture the behaviour of cemented soil. k is a curvature parameter, and ε_{ref} is a characteristic reference strain value for normalizing the damage strain. When $\varepsilon_d = \varepsilon_{ref}$, the current bond strength is equal to $\frac{p_{b0}}{e}$, where e is the Euler number. According to Figure 2, the curves with different k values pass the points (ε_{ref}, $\frac{p_{b0}}{e}$). Hence, ε_{ref} in addition to k must be used to control the overall degradation rate of p_b.

Elastic moduli

According to equation (2), K and G_0 are required to compute the incremental elastic strains. For the elastic moduli of uncemented soil, the mean stress and void ratio are usually incorporated (Oztoprak and Bolton, 2013; Zhou and Ng, 2015). Cementing bonds can further affect soil stiffness (Lo and Wardani, 2002). So far, several equations have been proposed (Pestana and Salvati, 2006; Trhlíková et al., 2012) to calculate the G_0 of cemented soil. However, they cannot reasonably predict G_0 under low and tensile stress conditions, which are quite common in cemented soil. Some equations, such as Trhlíková et al. (2012), predict a

negative G_0 value when subjected to tensile stress. The following equation is proposed to solve this problem based on Zhou et al. (2015):

$$G_0 = A(1+e)^{-1.3}\left(\left(\frac{p'+p_b}{p_r}\right)^{0.5} + n_c\left(\frac{p_b}{p_r}\right)^{0.5}\right) \quad (11)$$

where A and n_c are soil parameters for describing the shear modulus of cemented soil; e is the void ratio; and p_r is a reference pressure taken as 100 kPa here. There are two parameters in equation (11): A and n_c. Their influence on the predicted G_0 value is shown in Figure 3. The test result of cemented Monterey sand treated with Type I Portland cement (Saxena et al., 1998) is included for comparison. As shown in Figure 3(a), the computed G_0 value increases with increasing A. The computed curves at different A values are parallel at a given n_c. In addition, the incremental rate of G_0 with increasing stress is lower at a higher cement content, consistent with experimental results (Saxena et al., 1988; Pestana and Salvati, 2006; Trhlíková et al., 2012). The computed results at different n_c values are shown in Figure 3(b). n_c represents the sensitivity of G_0 to the cementation. When n_c is larger, G_0 is more sensitive to p_b.

In addition, the bulk modulus K is defined by G_0 and Poisson's ratio v in equation (12):

$$K = \frac{2(1+v)}{3(1-2v)}G_0 \quad (12)$$

Critical state and state parameter

The critical state line (CSL) is an important reference state in a state-dependent constitutive model (Ng et al., 2020). The cementation bonds are assumed to have been fully destroyed (i.e. $p_b = 0$) when the soil reaches a critical state. Projections of the CSL in the p'-q plane is modelled as a straight line:

$$q = M_c p' \quad (13)$$

where M_c is the stress ratio at the critical state, which can be determined from the critical state friction angle.

Projections of the CSL on the e-lnp' plane is described by the following equation:

$$\begin{cases} e_{cs} = \Gamma_c - \lambda \ln\left(\frac{1\ kPa}{p_r}\right) & \left(p' \leq 1\ kPa\right) \\ e_{cs} = \Gamma_c - \lambda \ln\left(\frac{p'}{p_r}\right) & \left(p' > 1\ kPa\right) \end{cases} \quad (14)$$

where Γ_c is the intercept of the CSL on the *e*-*ln p*' plane at the reference pressure of cemented soil; λ is the gradient of the CSL on the *e*-*ln p*' plane. This equation predicts a bilinear relationship between *e* and *ln p*', mainly because experimental studies in the literature (Papadopoulou and Tika, 2008) show that the critical state void ratio does not change significantly with *ln p*' when the effective mean stress is relatively low. In the current study, when $p' \leq 1\ kPa$, the critical state void ratio is assumed to be constant for simplicity.

The influence of cement content on the CSL has attracted great attention. Existing data generally show that M_c and Γ_c increases with increasing cement content (Schnaid et al., 2001; Wang and Leung, 2008; Mohsin, 2008; Subramaniam et al., 2016; Zhang et al., 2023). The increase is likely because cementing particles are still attached to soil particles/clusters at the critical state, increasing the roughness of particle/cluster surfaces and resulting in different particle packing modes (Wang and Leung, 2008). The observed changes in CSL are also likely related to strain localization. Cemented soils are more prone to strain localization than uncemented soils (Rinaldi and Santamarina, 2008; Jiang et al., 2011), obscuring the path to attaining CSL. Given the above considerations, the current model adopts the method of Zhang et al. (2023) to model a linear increase in M_c and Γ_c with cement content:

$$M_c = M_U + k_M C_c \quad (15)$$

$$\Gamma_c = \Gamma_U + k_\Gamma C_c \quad (16)$$

where M_U and Γ_U are the critical state stress ratio and void ratio of uncemented soil, respectively. k_M and k_Γ are non-negative model constants, respectively, controlling the changes in critical state stress ratio and void ratio with cement content. It should be highlighted that the current model incorporates the variation of CSL with cement content. If the cement content of one soil does not affect CSL, its behaviour can also be simulated with $k_M = 0$ and

$k_\Gamma = 0$.

Based on these critical state formulations, a state parameter (Ψ) (Been and Jefferies, 1985) is defined in equation (17). It refers to the difference between the current void ratio e and e_c with the same values of p':

$$\Psi = e - e_c \tag{17}$$

The values of Ψ are positive and negative for the soil state on the wet and dry sides of the CSL, respectively.

State-dependent dilatancy

Following Li (2002), the dilatancy is determined by equation (18):

$$D = \frac{d_0}{M_c}\left(M_d \left(\frac{\bar{\rho}_s}{\rho_s}\right)^{0.5} - \eta_c\right) \tag{18}$$

$$M_d = M_c exp(n_d \Psi) \tag{19}$$

where d_0 and n_d are soil parameters, η_c is the stress ratio defined as $\eta_c = q/(p' + p_b)$, M_d is the stress ratio at which phase transformation occurs under the preliminary shearing (Zhou et al. 2020). Phase transformation is the transition of soil behaviour from contractive to dilative during shearing (Ishihara et al., 1975). To account for the effects of loading and unloading history on the shear behaviour, equation (19) incorporates the term $\sqrt{\frac{\bar{\rho}_s}{\rho_s}}$. In the case of primary shearing, $\sqrt{\frac{\bar{\rho}_s}{\rho_s}} = 1$.

As discussed earlier, the dilatancy tendency increases with increasing cement content. This behaviour can be modelled by equation (18), governed by an upward shift of the critical state line in the $v - \ln p'$ plane with increasing cement content. A larger Γ_c value results in a smaller Ψ and a lower M_d. Consequently, the phase transformation occurs at an earlier shearing stage and a higher dilatation value.

Hardening law and condition of consistency

The loading index Λ in equation (3) is determined using the condition of consistency and

hardening law. In this model, the evolution of the bounding surface *Fs* directly depends on the plastic deviator and volumetric strains. During the primary shearing, when yielding is occurring with the stress state on *Fs*, the condition of consistency suggests that:

$$\frac{\partial F_S}{\partial p'}dp' + \frac{\partial F_S}{\partial q}dq + \frac{\partial F_S}{\partial p_b}\frac{\partial p_b}{\partial \varepsilon_q^p}d\varepsilon_q^p + \frac{\partial F_S}{\partial p_b}\frac{\partial p_b}{\partial \varepsilon_v^p}d\varepsilon_v^p + \frac{\partial F_S}{\partial M_m}\frac{\partial M_m}{\partial \varepsilon_q^p}d\varepsilon_q^p = 0 \tag{20}$$

The plastic modulus K_p is introduced and defined in equation (21). The evolution of the boundary surface F_S during the shearing process is controlled by M_m and p_b.

$$K_p = -\left(\frac{\partial F_S}{\partial p_b}\frac{\partial p_b}{\partial \varepsilon_q^p} + \frac{\partial F_S}{\partial p_b}\frac{\partial p_b}{\partial \varepsilon_v^p}D + \frac{\partial F_S}{\partial M_m}\frac{\partial M_m}{\partial \varepsilon_q^p}\right) \tag{21}$$

By substituting equations (4) to (21), the value of Λ can be determined by equation (22).

$$\Lambda = \frac{1}{K_p}\left(\frac{\partial F_S}{\partial p'}dp' + \frac{\partial F_S}{\partial q}dq\right) = \frac{1}{K_p}(dq - M_m dp') \tag{22}$$

To calculate K_p, $\frac{\partial F_S}{\partial p_b}$ can be obtained by differentiating equation (4):

$$\frac{\partial F_S}{\partial p_b} = -M_m \tag{23}$$

where $\frac{\partial p_b}{\partial \varepsilon_q^p}$ and $\frac{\partial p_b}{\partial \varepsilon_v^p}$ are function of dp_b and dε_q^p by differentiating equations (9) and (10):

$$\frac{\partial p_b}{\partial \varepsilon_q^p} = -p_{b0}\exp\left(-\left(\frac{\varepsilon_d}{\varepsilon_{ref}}\right)^k\right)\mathrm{k}\left(\frac{\varepsilon_d}{\varepsilon_{ref}}\right)^{k-1}\frac{1}{\varepsilon_{ref}\sqrt{1+D^2}} \tag{24a}$$

$$\frac{\partial p_b}{\partial \varepsilon_v^p} = -p_{b0}\exp\left(-\left(\frac{\varepsilon_d}{\varepsilon_{ref}}\right)^k\right)\mathrm{k}\left(\frac{\varepsilon_d}{\varepsilon_{ref}}\right)^{k-1}\frac{\mathrm{D}}{\varepsilon_{ref}\sqrt{1+D^2}} \tag{24b}$$

The term $\frac{\partial F_S}{\partial M_m}\frac{\partial M_m}{\partial \varepsilon_q^p}$ corresponding to the influence of the shearing mechanism on the stress ratio M_m. In the study of Zhou et al. (2015), the change of M_m induced by shear was simplified, which is only related to the plastic deviatoric strain. Referring to Zhou et al. (2015), $\frac{\partial M_m}{\partial \varepsilon_q^p}$ is defined as follows for simplicity:

$$\frac{\partial F_S}{\partial M_m}\frac{\partial M_m}{\partial \varepsilon_q^p} = \frac{hG}{M_m}\left(M_b\frac{\overline{\rho_s}}{\rho_s} - M_m\right) \tag{25}$$

According to equations (23) through (25), the plastic modulus K_p can be obtained:

$$K_p = \frac{hG}{M_m}\left(M_b\frac{\overline{\rho_s}}{\rho_s} - M_m\right) - M_m p_b\exp\left(-\left(\frac{\varepsilon_d}{\varepsilon_{ref}}\right)^k\right)\mathrm{k}\left(\frac{\varepsilon_d}{\varepsilon_{ref}}\right)^{k-1}\frac{\sqrt{1+D^2}}{\varepsilon_{ref}} \tag{26}$$

Calibration of model parameters

In total, 16 parameters are needed in the proposed model, as shown in Table 1. 10 of them were adopted in the reference model proposed by Zhou et al. (2015) for uncemented soil, and they can be calibrated following the method of Zhou et al. (2015). Seven new parameters are used in the proposed model to simulate cementation effects, and they can be determined using the following methods:

(1) Parameters k_M and k_Γ describe the effects of cement content on the stress ratio and void ratio at the critical state. To calibrate k_M, it is necessary to measure the critical stress ratio M_c through triaxial shear tests at different cement contents Cc. Then, the relationship between M_c and Cc is fitted using equation (15) to determine k_M. Similarly, k_Γ can be obtained by fitting the relationship between Γ_c and Cc with equation (16).

(2) Parameters k_{pb} and β can be calibrated using the results of unconfined compressive tests at different cement contents. Given the assumption that the cementation strength does not decrease before reaching peak strength, the initial bond strength p_{b0} can be approximated as follows:

$$p_{b0} = \frac{q_u(3-M_c)}{3M_c} \tag{27}$$

where q_u is the unconfined compressive strength. The measured relationship between p_{b0} and Cc can be fitted using equation (8) to determine the value of k_{pb} and β.

(3) The remaining two parameters, ε_{ref} and k, are calibrated based on the relationship between bond strength and damage strain. According to Figure 2, ε_{ref} is the damage strain at which p_b equals to p_{b0} divided by e. If the $p_b - \varepsilon_d$ relationship is not available, an alternative approach is to use the relationship between axial stress σ_{axial} and axial strain ε_{axial} from the softening section of unconfined compression tests. This approximation assumes that the $p_b - \varepsilon_d$ and $\sigma_{axial} - \varepsilon_{axial}$ relationships exhibit similar behaviour, based on the following three features: (i) the total strain closely approximates the plastic strain during

the softening process; (ii) the volumetric strain in unconfined compression tests is typically small, resulting in similar axial, deviatoric, and damage strains; (iii) the values of $\frac{p_b}{p_{bo}}$ and $\frac{\sigma_{axial}}{q_u}$ in the softening process of unconfined compression tests are close. In this alternative method, ε_{ref} is estimated as the axial strain corresponding to the point where the axial stress decreases to q_u/e during the strain-softening process. Once ε_{ref} is determined, k can be estimated by fitting the $p_b - \varepsilon_d$ or $\sigma_{axial} - \varepsilon_{axial}$ curve using equation (10).

Model validation

Elastic shear modulus

Saxena et al. (1988) studied the elastic moduli of Monterey No. 0 sand treated with Type I Portland cement by resonant column tests. The calculated and measured results of G_0 at different stress conditions are compared. As shown in Figure 4, in the log G_0 – log p' plane, G_0 increases linearly with increasing p'. The incremental rate is smaller for higher cement content, demonstrating coupling effects between the stress and cementing bonds on G_0. In equation (11), the term $\left(\frac{p'+p_b}{p_r}\right)^{0.5} + n_c {p_b}^{0.5}$ is used to account for the coupling effects of stress and cementation. At a larger p_b value, the role of stress becomes relatively less important.

Yang (2008) investigated the effect of void ratio on the elastic shear modulus of cemented sand through bender element and resonant column tests. Their study used type III Portland Cement to stabilize Puerto Rico sand. Figure 5 compares the measured and calculated results at three relative densities (Dr = 60%, Dr = 80%, Dr = 100%). The calculated results are determined using equation (11) with the parameters shown in Figure 5. In the log G_0 - e plane, G_0 decreases linearly with an increasing void ratio, and the decremental rate is almost independent of cement content. At a given void ratio, G_0 increases with increasing cement content. The above behaviour is well captured by equation (11).

To further demonstrate the capability of equation (11), this study compares the computed

and measured G_0 results of isotropic compression tests on kaolin clay treated with 4% ordinary Portland cement. The test results are obtained from Trhlíková et al. (2012) and shown in Figure 6. Equation (11) gives a good prediction for the uncemented specimen. For the cemented clay, the equation does not capture the experimental results well in the stress range of 100 to 1000 kPa. The discrepancies are likely because the proposed model predicts an elastic soil behaviour during isotropic compression for simplicity, as illustrated above. Hence, the degradation of bonding during isotropic compression cannot be considered.

Stress-strain relation and dilatancy during drained shearing

Marri et al. (2012) conducted triaxial drained shear tests on Portaway sand at different Ordinary Portland Cement contents (5, 10, 15%) and confining pressures (1, 4, 8, 12 MPa). The relative densities of the three specimens were 88%, 82% and 79% at cement contents of 5%, 10% and 15%, respectively. A wide range of high stress is simulated for two reasons. Firstly, cemented soils may be subjected to high stress in some engineering problems, such as deep pile foundations, especially offshore piling, deep mine shafts, high earth dams and deep oil-bearing strata (Marri et al., 2012). Secondly, the model performance over a wide stress range can be evaluated.

The model parameters are calibrated and shown in Table 1. Figure 7 compares the measured and computed results. It should be noted that Marri et al. (2012) only reported the axial strain and volume change (equivalent to volumetric strain). With the assumption of fully saturated specimens, deviatoric strain (ε_q) is calculated from the measured volumetric strain (ε_v) and axial strain (ε_1) using the following two equations:

$$\varepsilon_q = \frac{2(\varepsilon_1 - \varepsilon_3)}{3} \tag{28}$$

$$\varepsilon_v = \varepsilon_1 + 2\varepsilon_3 \tag{29}$$

where ε_3 is the radial strain. The proposed model can well capture the stress-strain and volume change behaviour during shearing. The cemented sand exhibits clear strain-softening

behaviour when the confining pressure is relatively low. This behaviour is because p_b plays a dominant role, and the peak strength is higher than the critical state shear strength. On the contrary, under higher confining pressure, the role of p_b is overweighted by that of p'. Cementation bonds have been fully degraded before reaching the peak state, so a strain-hardening behaviour is observed.

With an increase in cement content, strain-softening is more obvious. This increase is because the p_b value increases with the cement content, which leads to the failure bounding surface in Figure 1 shifting towards the left. Furthermore, with the increase in cement content, the soil becomes slightly more dilative. This trend is captured by the model, mainly due to the upward movement of the critical state line in *e-lnp′* plane, in equation (14). A larger Γ_c value results in smaller Ψ and M_d, leading to earlier phase transformation and higher dilatancy.

Stress-strain relation and effective stress path during undrained shearing

Horpibulsuk et al. (2004) studied cementation effects on clay improved using Type I Portland cement through undrained triaxial tests. Isotopically consolidated undrained triaxial compression tests were conducted on specimens with 6% cement content after 28 days of curing. It revealed that the cementation enhances the strain-softening behaviour. Figure 7 compares the calculated results and measured data. The calibrated parameters are summarized in Table 1. In undrained shear tests with $\varepsilon_v = 0$, the radial and deviatoric strains can be calculated by the measured axial strain, using equations (28) and (29).

As shown in Figure 9, the stress path of cemented soil exceeds the CSL due to cementation. After reaching the peak shear strength, the specimens exhibit strain-softening behaviour due to the destruction of cementation bonds, and then the strength degrades to the CSL. The proposed model well captures this behaviour with some differences, mainly at the cement content of 12%. The discrepancy between the computed and measured results may be because cementation effects on the dilatancy are modelled in a simplified and indirect approach (i.e., considering

the effects of cementation on the state parameter in Eqs. (18) and (19)). Cementation may alter dilatancy by other mechanisms (e.g., the changes in soil particle number and fabric) (Martinez and DeJong, 2009; Rios et al., 2012). Some advanced flow rules could be used to improve the modelling of the dilation behaviour, such as bond strength-dependent dilatancy (e.g. Horpibulsuk et al., 2010).

Stiffness at very small strains and small strains

Yao (2017) studied the elastic shear modulus G_0 and its degradation curves of cemented Singapore marine clay with different Ordinary Portland Cement contents and confining pressures. Figure 10 compares the measured and calculated secant modulus result. The secant modulus is the ratio of q to $3\varepsilon_q$, where q and ε_q are shear stress and deviator strain, respectively. The calibrated parameters are summarised in Table 1.

As shown in Figure 10, the elastic shear modulus in the very small strain range (< 0.001%) is accurately modelled under different confining pressures. The good performance can be mainly because equation (11) can reasonably consider the effect of effective mean stress and cementation on the elastic shear modulus. In addition, there are some minor differences between the measured and computed results, probably because equation (10) models the relationship between bond strength (p_{b0}) and cement content in a simplified approach. It underestimates the p_{b0} value at relatively lower cement content and overestimates the p_{b0} value at relatively higher cement content.

The degradation curves of the secant shear modulus in the small strain range (0.001% – 1%) are well captured, attributed to two merits of the models: (i) the elastic shear modulus can be determined accurately using equation (11); (ii) equation (10) reasonably characterises the degradation of p_b. These two aspects are important to predicting shear modulus at very small strains and modelling shear modulus degradation at small strains. They were not fully incorporated into existing models for cemented soil.

Mechanical behaviour of cemented soil from small to large strains

Marques et al. (2021) conducted triaxial tests to study cemented sand's strength and small strain stiffness behaviour. Early-strength Portland cement (Type III) was the binder to shorten the test duration. The measured and calculated results are compared in Figure 11. The calibrated parameters are summarised in Table 1. The influence of parameter k, in equation (11), on the small strain stiffness degradation curve is studied. As shown in Figure 11, in the case of k = 4 and k_{pb} = 18, both the stress-strain curve and the degradation curve of small strain stiffness are well captured. The case with k = 1, which is a common assumption in existing models, predicts a faster and slower degradation before and after ε_{ref} than the case with k = 4, respectively, as shown in Figure 2. With k = 1, a larger p_{b0} is required to capture the peak strength of cemented soil. When k = 1, k_{pb} = 32 is required for modelling the peak strength, but this overestimates the small strain stiffness. In other words, if k = 1 is assumed, it is challenging to predict the behaviour of cemented soil over a wide strain range well. In addition, there are some obvious differences between the measured and computed volumetric strains, as shown in Figure 11(c). This limitation is likely because the influence of cement content on dilatancy is modelled in a simplified approach, as discussed above. Moreover, cemented soils often exhibit strain localization during shearing, especially during softening (shear strain > 1% in Figure 11). The specimen is not an ideal representative element, causing differences between the measured and computed results at strains above 1%.

Consoli et al. (2000) conducted triaxial tests on cemented and weathered sandstone with 3% cement content. The results are used for further validating the proposed model. The calibrated parameters are summarised in Table 1. Figure 12 shows the measured and computed results. Overall, the model prediction curve and the test results show consistent trends. There are some discrepancies between the computed and measured results. This limitation is likely because the current model adopts a linear failure bounding surface (see equation (5)) for

simplicity, while the failure envelope of cemented soils can be highly nonlinear (Wu et al., 2017; Sharma et al., 2011).

Stress-strain behaviour during the loading and reloading process

Unlike the classical elastoplastic theory, which assumes elastic soil behaviour within the yield surface, the bounding surface plasticity theory allows for gradual yielding when the stress path is inside the boundary surface. The two theories are compared to simulate a laboratory test reported by Mohsin (2008). Calcareous sediment treated with 10% gypsum was tested in triaxial apparatus at an effective confining pressure of 600 kPa. A specimen was subjected to three cycles of deviatoric stress. The measured and computed results are shown in Figure 13. The experimental results clearly show gradual yielding and irreversible deformation during reloading. Furthermore, the specimen failed during reloading even though the deviatoric stress did not exceed the maximum deviatoric stress applied during the first loading. The failure is mainly attributed to the degradation of bond strength. The bounding surface plasticity model can well capture these phenomena. In contrast, soil responses during the unloading and reloading processes are reversible when the classical elastoplasticity framework is used. The above features cannot be simulated.

Summary and conclusions

Based on the bounding surface plasticity theory, a new state-dependent model is developed to simulate the cemented soil behaviour at both small and large strains. The size and position of the bounding surface are modified to incorporate the cementation effects. Some new equations are proposed to improve the modelling of the small strain behaviour of cemented soil, such as (i) the elastic shear modulus under both tensile and compressive stress conditions; (ii) the non-linear degradation of bonding strength (p_b) with damage strain (ε_d) in the $ln\, p_b - \varepsilon_d$ plane. Seven new parameters are added to simulate the behaviour of cemented soil. These parameters can be calibrated based on laboratory tests. For the convenience of engineering

design, the value of some model parameters is correlated with cement content.

The model has been used to predict the behaviour of cemented soils at both small and large strains. The computed results are compared with the experimental results of cemented sands and clays along various stress paths.

The proposed models have several key advantages. Firstly, it can accurately capture the stiffness degradation behaviour of cemented soil in the small strain range. Secondly, the use of bounding surface plasticity theory allows it to well simulate nonlinear soil behaviour during unloading and reloading. Thirdly, the strain softening behaviour is well simulated based on the newly proposed bonding degradation equation. The proposed model is expected to improve the analysis of the serviceability limit state of infrastructures involving cemented soil.

In further studies, this model could be further improved based on more experimental results. Some additional features of cemented soil behaviour may be incorporated, such as the nonlinearity of failure envelopes and the bond strength-dependent dilatancy.

Acknowledgements

The National Science Foundation of China supports this work through research grant 52022004. The authors also would like to thank the HKSAR Research Grants Council (RGC) for providing financial support through grant 15205721 and the Shenzhen Science and Technology Innovation Commission through grant 2022N040.

Data availability statement

All data, models, and code generated or used during the study appear in the submitted article.

References

Acar, Y. B. and Eltahir, E. A. 1986. “Low Strain Dynamic Properties of Artificially Cemented Sand.” *J. Geotech. Eng.* 112 (11): 1001-1015.

Atkinson, J. 2000. “Non-linear soil stiffness in routine design.” *Géotechnique* 50 (5): 487-508.

497 Baudet, B. and Stallebrass, S. 2004. “A constitutive model for structured clays.” *Géotechnique*
498 54 (4): 269-278.
499 Been, K. and Jefferies, M. G. 1985. “A state parameter for sands.” *Géotechnique* 35 (2): 99-
500 112.
501 Clough, G. W., Sitar, N., Bachus, R. C. and Rad, N. S. 1981. “Cemented sands under static
502 loading.” *J. Geotech. Eng. Div.* 107 (6): 799-817.
503 Consoli, N., Rotta, G. and Prietto, P. 2000. “Influence of curing under stress on the triaxial
504 response of cemented soils.” *Géotechnique* 50 (1): 99-105.
505 Consoli, N. C., Foppa, D., Festugato, L. and Heineck, K. S. 2007. “Key parameters for strength
506 control of artificially cemented soils.” *J. Geotech. Geoenviron. Eng.* 133 (2): 197-205.
507 Cuccovillo, T. & Coop, M. 1999. “On the mechanics of structured sands.” *Géotechnique*
508 49(6):741-760.
509 Dafalias, Y. F. 1986. “Bounding surface plasticity. I: Mathematical foundation and
510 hypoplasticity.” *J. Eng. Mech.* 112 (9): 966-987.
511 Dafalias, Y. F. and Manzari, M. T. 2004. “Simple plasticity sand model accounting for fabric
512 change effects”. *J. Eng. Mech.* 130(6):622-634.
513 Doherty, J. P. and Wood, D. M. 2020. “A bonding and damage constitutive model for lightly
514 cemented granular material.” *Comput. Geotech.,* 127: 103732.
515 Fernandez, A. L., and Santamarina, J. C. 2001. “Effect of cementation on the small-strain
516 parameters of sands.” *Can. Geotech. J.* 38(1), 191-199.
517 Hirai, H., Takahashi, M. and Yamada, M. 1989. “An elastic-plastic constitutive model for the
518 behaviour of improved sandy soils.” *Soils Found.* 29 (2): 69-84.
519 Horpibulsuk, S., Liu, M. D., Liyanapathirana, D. S. and Suebsuk, J. 2010. “Behaviour of
520 cemented clay simulated via the theoretical framework of the Structured Cam Clay model.”
521 *Comput. Geotech.* 37 (1-2): 1-9.

522 Horpibulsuk, S., Miura, N. and Bergado, D. 2004. “Undrained shear behaviour of cement
523 admixed clay at high water content.” *J. Geotech. Geoenviron. Eng.* 130 (10): 1096-1105.
524 Ishihara, K., Tatsuoka, F., and Yasuda, S. (1975). “Undrained deformation and liquefaction of
525 sand under cyclic stresses.” *Soils Found*, 15(1), 29-44
526 Kamruzzaman, A., Chew, S. and Lee, F. 2009. “Structuration and destructuration behaviour of
527 cemented Singapore marine clay.” *J. Geotech. Geoenviron. Eng.* 135 (4): 573-589.
528 Li, X. 2002. “A sand model with state-dapendent dilatancy.” *Géotechnique* 52 (3): 173-186.
529 Manzari, M. T. and Dafalias, Y. F. 1997. “A critical state two-surface plasticity model for sands.”
530 *Géotechnique* 47(2):255-272.
531 Marques, S. F. V., Festugato, L. and Consoli, N. C. 2021. “Stiffness and strength of an
532 artificially cemented sand cured under stress.” *Granul. Matter* 23 (2): 1-16.
533 Marri, A., Wanatowski, D. and Yu, H. 2012. “Drained behaviour of cemented sand in high
534 pressure triaxial compression tests.” *Geomech. Geoeng.* 7 (3): 159-174.
535 Martinez, B. C., and DeJong, J. T. 2009. “Bio-mediated soil improvement: load transfer
536 mechanisms at the micro-and macro-scales.” *In Advances in ground improvement:*
537 *research to practice in the United States and China* (pp. 242-251).
538 Melentijevic, S., Arcos, J. and Oteo, C. 2013. “Application of cement deep mixing method for
539 underpinning.” *In Proceedings of the 18th International Conference on Soil Mechanics*
540 *and Geotechnical Engineering*, pp. 2549-2552.
541 Mohsin, A. (2008) *Automated Gmax measurement to explore degradation of artificially*
542 *cemented carbonate sand*. Australia: University of Sydney.
543 Nweke, C. 2017. *Constitutive Modeling of Weakly Cemented Sands.* University of California,
544 Berkeley.
545 Namikawa, T. and Mihira, S. 2007. “Elasto- plastic model for cement- treated sand.” *Int. J.*
546 *Numer. Anal. Methods. Geomech.* 31 (1): 71-107.

547 Ng, C. W. W., Zhou, C., and Chiu, C. F. (2020). "Constitutive modelling of state-dependent
548 behaviour of unsaturated soils: an overview". *Acta Geotechnica*, 15, 2705-2725.
549 Nguyen, L., Fatahi, B. and Khabbaz, H. 2017. "Development of a constitutive model to predict
550 the behaviour of cemented clay during cementation degradation: C3 model." *Int. J.*
551 *Geomech.* 17 (7): 04017010.
552 Nguyen, L. D., Fatahi, B. and Khabbaz, H. 2014. "A constitutive model for cemented clays
553 capturing cementation degradation." *Int. J. Plast.* 56: 1-18.
554 Ni, L., Suleiman, M. T., and Raich, A. 2016. "Behaviour and soil–structure interaction of
555 pervious concrete ground-improvement piles under lateral loading." *J. Geotech.*
556 *Geoenviron. Eng.*, 142(2): 04015071.
557 Oztoprak, S. and Bolton, M. 2013. "Stiffness of sands through a laboratory test database."
558 *Géotechnique* 63 (1): 54-70.
559 Papadopoulou, A., & Tika, T. 2008. "The effect of fines on critical state and liquefaction
560 resistance characteristics of non-plastic silty sands." *Soil Foun*, 48(5), 713-725.
561 Pestana, J. M. and Salvati, L. A. 2006. "Small-strain behaviour of granular soils. I: Model for
562 cemented and uncemented sands and gravels." *J. Geotech. Geoenviron. Eng.* 132 (8):
563 1071-1081.
564 Pongsivasathit, S., Petchgate, W., Horpibulsuk, S. and Piyaphipat, S. 2021. "Composite
565 contiguous pile wall and deep mixing column wall as a dam–Design, construction and
566 performance." *Case Stud. Constr. Mater.* 15, e00771.
567 Ravanbakhsh, E. and Hamidi, A. 2013. "Development of a generalised plasticity constitutive
568 model for cemented sands using critical state concepts." *Int. J. Geotech. Eng.* 7 (4): 364-
569 373.
570 Rios, S., Viana da Fonseca, A. and Baudet, B. A. 2012. "Effect of the porosity/cement ratio on
571 the compression of cemented soil." *J. Geotech. Geoenviron. Eng.*, 138(11), 1422-1426.

572 Rouainia, M., and Muir Wood, D. 2000. "A kinematic hardening constitutive model for natural
573 clays with loss of structure." *Géotechnique*, 50(2), 153-164.
574 Sasanian, S. 2011. *The behaviour of cement stabilised clay at high water contents*. The
575 University of Western Ontario.
576 Saxena, S. K., Avramidis, A. S. and Reddy, K. R. 1988. "Dynamic moduli and damping ratios
577 for cemented sands at low strains." *Can. Geotech. J*., 25 (2): 353-368.
578 Schnaid, F., Prietto, P. D., and Consoli, N. C. 2001. "Characterisation of cemented sand in
579 triaxial compression." *J. Geotech. Geoenviron. Eng.*, 127 (10): 857-868.
580 Sharma, M. R., Baxter, C. D., Hoffmann, W., Moran, K. and Vaziri, H. (2011) Characterization
581 of weakly cemented sands using nonlinear failure envelopes. *Int J. Rock Mech.*
582 *Min.*,48(1):146-151.
583 Subramaniam, P., Sreenadh, M. M. and Banerjee, S. 2016. "Critical state parameters of dredged
584 Chennai marine clay treated with low cement content." *Mar. Georesour. Geotechnol.* 34
585 (7): 603-616.
586 Suebsuk, J., Horpibulsuk, S. and Liu, M. D. 2010. "Modified Structured Cam Clay: A
587 generalised critical state model for destructured, naturally structured and artificially
588 structured clays." *Comput. Geotech.* 37 (7-8): 956-968.
589 Taiebat, M. and Dafalias, Y. F. (2008) "SANISAND: Simple anisotropic sand plasticity model."
590 *Int. J. Numer. Anal. Met.* 32(8):915-948.
591 Trhlíková, J., Mašín, D. and Boháč, J. 2012. "Small-strain behaviour of cemented soils."
592 *Géotechnique* 62 (10): 943-947.
593 Vatsala, A., Nova, R. & Murthy, B. S. (2001) Elastoplastic model for cemented soils. *J. Geotech.*
594 *Geoenviron. Eng.* 127(8):679-687.
595 Voottipruex, P., Jamsawang, P., Sukontasukkul, P., Jongpradist, P., Horpibulsuk, S. and
596 Chindaprasirt, P. 2019. "Performances of SDCM and DCM walls under deep excavation

597 in soft clay: Field tests and 3D simulations." *Soils Found.* 59 (6): 1728-1739.
598 Wang, G. annd Xie, Y. 2014 "Modified bounding surface hypoplasticity model for sands under
599 cyclic loading." *J. Eng. Mech.* 140(1):91-101.
600 Wang, Y. and Leung, S. 2008. Characterisation of cemented sand by experimental and
601 numerical investigations." *J. Geotech. Geoenviron. Eng.* 134 (7): 992-1004.
602 Wang, Z. L., Dafalias, Y. F. and Shen, C. K. 1990. "Bounding surface hypoplasticity model for
603 sand." *J. Eng. Mech.* 116 (5): 983-1001.
604 Watabe, Y. and Noguchi, T. 2011. "Site-investigation and geotechnical design of D-runway
605 construction in Tokyo Haneda Airport." *Soils Found.* 51 (6): 1003-1018.
606 Wu, S., Zhang, S., Guo, C. and Xiong, L. (2017) A generalized nonlinear failure criterion for
607 frictional materials. *Acta Geotech.* 12:1353-1371.
608 Xiao, H., Lee, F. H. and Chin, K. G. 2014. "Yielding of cemented marine clay." *Soils Found.*
609 54 (3): 488-501.
610 Xiao, H., Lee, F. H. and Liu, Y. 2017. "Bounding surface cam-clay model with cohesion for
611 cement-admixed clay." *Int. J. Geomech.* 17 (1): 04016026.
612 Yamada, S., Sakai, T., Nakano, M., and Noda, T. 2022. "Method to Introduce the Cementation
613 Effect into Existing Elastoplastic Constitutive Models for Soils." *J. Geotech. Geoenviron.*
614 *Eng.* 148 (5): 04022013.
615 Yang, L. 2008. *Shear stiffness modeling of cemented sand and cemented clay*. University Of
616 Notre Dame.
617 Yao, K. 2017. *Small strain behaviour of cement treated Singapore marine clay*. National
618 University of Singapore.
619 Yun, T. S. & Santamarina, J. C. 2005. "Decementation, softening, and collapse: changes in
620 small-strain shear stiffness in k 0 loading. " *J. Geotech. Geoenviron. Eng.* 131(3):350-
621 358.

622 Zhang, A., Dafalias, Y. F. and Jiang, M. 2023. “A bounding surface plasticity model for
623 cemented sand under monotonic and cyclic loading.” *Géotechnique*, 73(1), 44-61.
624 Zhou, C. and Ng, C. W. W. 2015. “A thermomechanical model for saturated soil at small and
625 large strains.” *Can. Geotech. J.* 52 (8): 1101-1110.
626 Zhou, C., Ng, C. W. W. and Chen, R. 2015. “A bounding surface plasticity model for
627 unsaturated soil at small strains.” *Int. J. Numer. Anal. Methods Geomech.* 39 (11): 1141-
628 1164.
629 Zhou, C. and Ng, C. W. W. 2016. “Simulating the cyclic behaviour of unsaturated soil at various
630 temperatures using a bounding surface model.” *Géotechnique* 66(4):344-350.
631 Zhou, C. and Ng, C. W. W. 2018. “A new thermo-mechanical model for structured soil.”
632 *Géotechnique*, 68(12), 1109-1115.
633 Zhou, C., Tai, P. and Yin, J. H. 2020. “A bounding surface model for saturated and unsaturated
634 soil- structure interfaces.” *Int. J. Numer. Anal. Methods Geomech.* 44 (18): 2412-2429.
635

Appendix

Plastic deviatoric and volumetric strains could induce the degradation of cementation. In previous models, the cementation degradation is often a function of damage strain, considering the influence of both strains. The damage strain in many models (Rouainia and Muir Wood, 2000; Baudet and Stallebrass, 2004; Zhou and Ng, 2018) can be unified using the following equation:

$$\varepsilon_d = \sqrt{(\alpha)\varepsilon_p^{p\,2} + (2-\alpha)\varepsilon_v^{p\,2}} \tag{30}$$

where α is a parameter that controls the relative importance of plastic deviatoric and volumetric strains on damage strain. To analyse the effects of α value on the model prediction, three different values (0.66, 1 and 1.33) are used to simulate the test results of Marque et al. (2021). It can be seen that the value of α has an obvious influence on the post-peak behaviour because the cement degradation is large in this strain range. However, the influence of α on the stress-strain relation and stiffness degradation before the peak state is minimal.

It should be pointed out that different values could be used in the constitutive modelling. If the α value changes, another parameter k of equation (9) should be re-calibrated. The proper combination of α and k values can give a reasonable prediction. Therefore, the current model assumes $\alpha = 1$ for simplicity.

Table 1. Summary of model parameters.

Parameter	Symbol	Portaway sand (Marri et al. 2012)	Ariake clay (Horpibulsuk et al. 2004)	Singapore marine clay (Yao 2017)	Osorio sand (Marques et al. 2021)	Weathered sandstone (Consoli et al. 2000)	Calcareous sediments, (Mohsin et al. 2008)
Elasticity	A (MPa)	200	150	280	380	500	200
	ν	0.1	0.1	0.1	0.1	0.1	0.2
	n_c	1.0	1.0	2.9	1.5	15.0	5.0
Critical state	M_U	1.20	1.58	0.90	1.32	1.39	1.40
	k_M	3.0	1.8	1.0	1.0	3.6	1.0
	λ	0.08	0.40	0.20	0.02	0.02	0.10
	Γ_U	2.1	4.8	3.0	2.8	1.7	3.0
	k_Γ	0.1	1.8	0.5	2.0	3.0	2.5
Flow rule	n_d	2	3	0.5	0.05	2.0	0.5
	d_0	1.2	0.1	0.5	3.0	0.1	0.3
Hardening law	n_b	2.0	1.0	1.0	0.5	0.8	0.3
	h	0.6	0.4	0.7	0.8	0.1	0.1
Cementation parameter	ε_{ref}	0.06	0.06	0.05	0.03	0.04	0.04
	k	2.0	2.0	2	4.0	2.0	3
	k_{pb} (MPa)	68	300	1.6	18	30	27
	β	6.0	2.6	1.5	1.5	1.6	2.0

Fig. 1

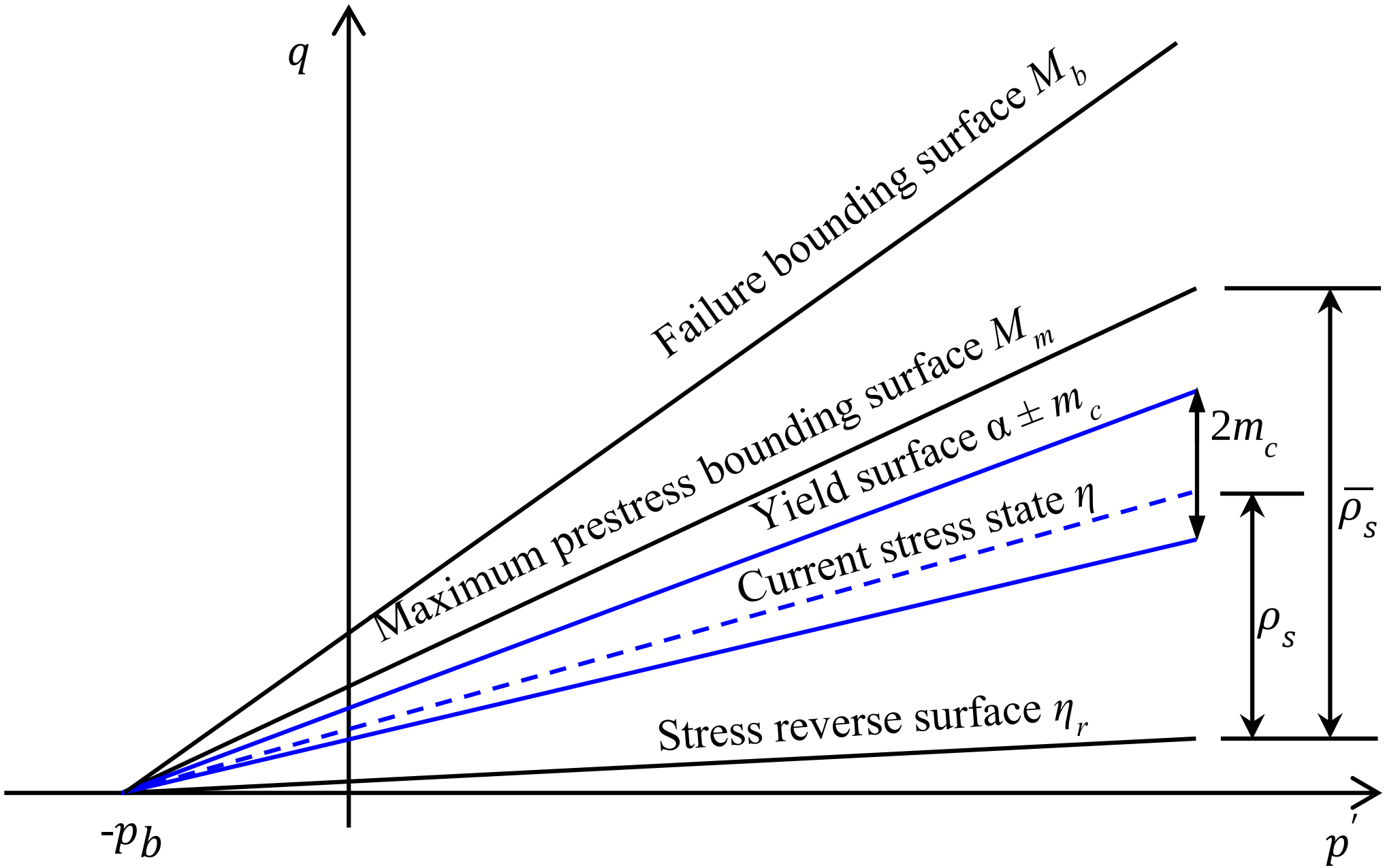

Fig. 2

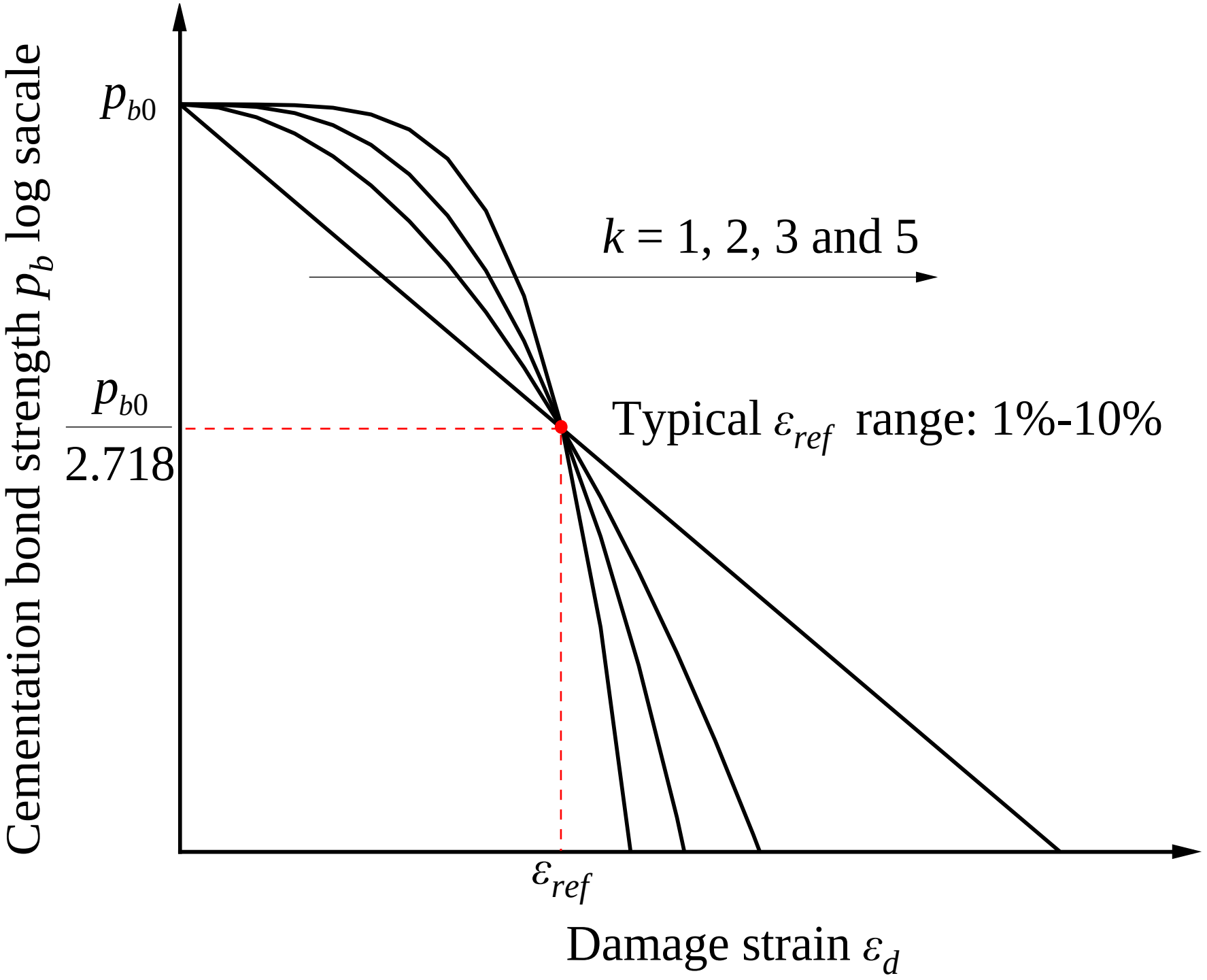

Fig. 3a

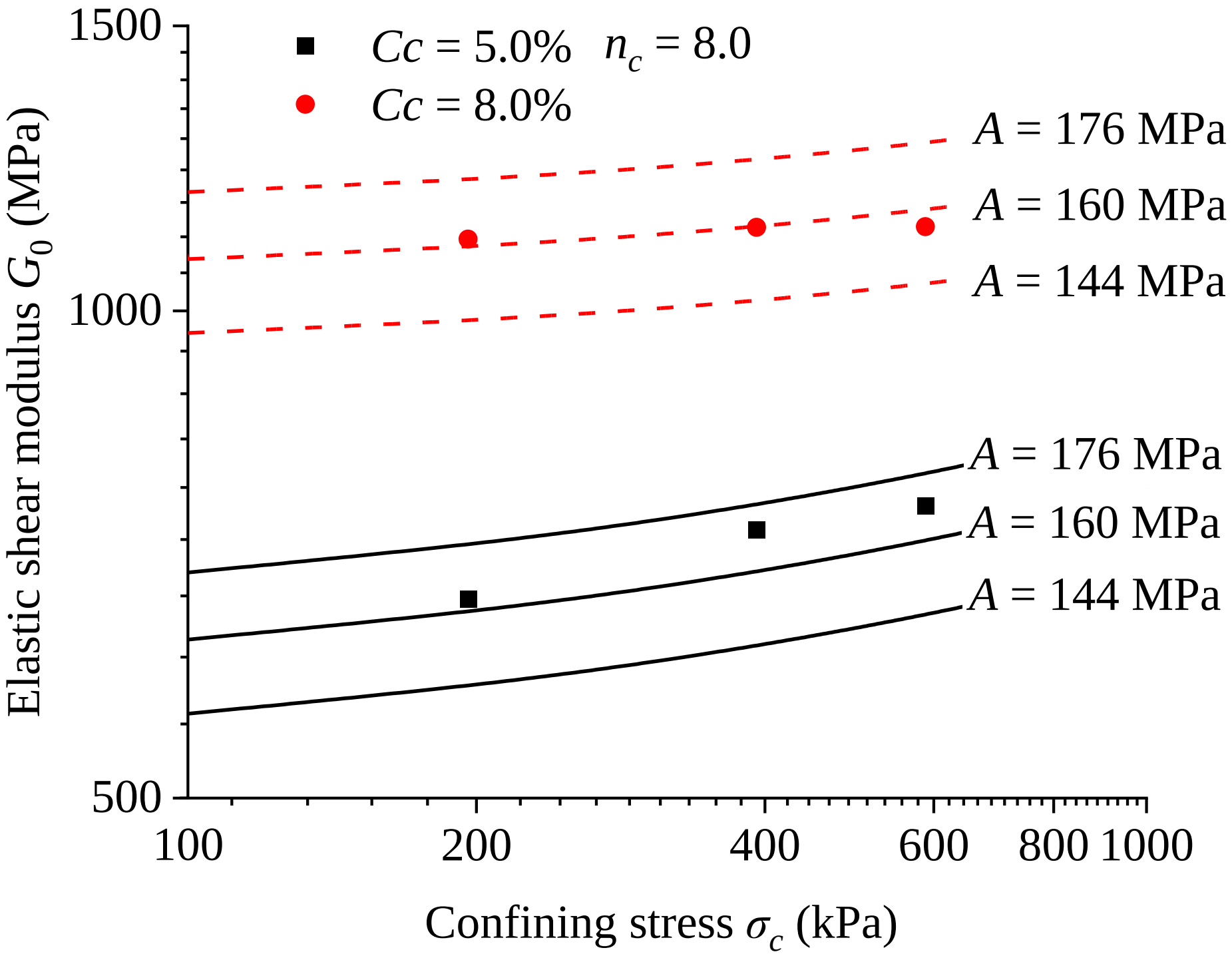

Fig. 3b

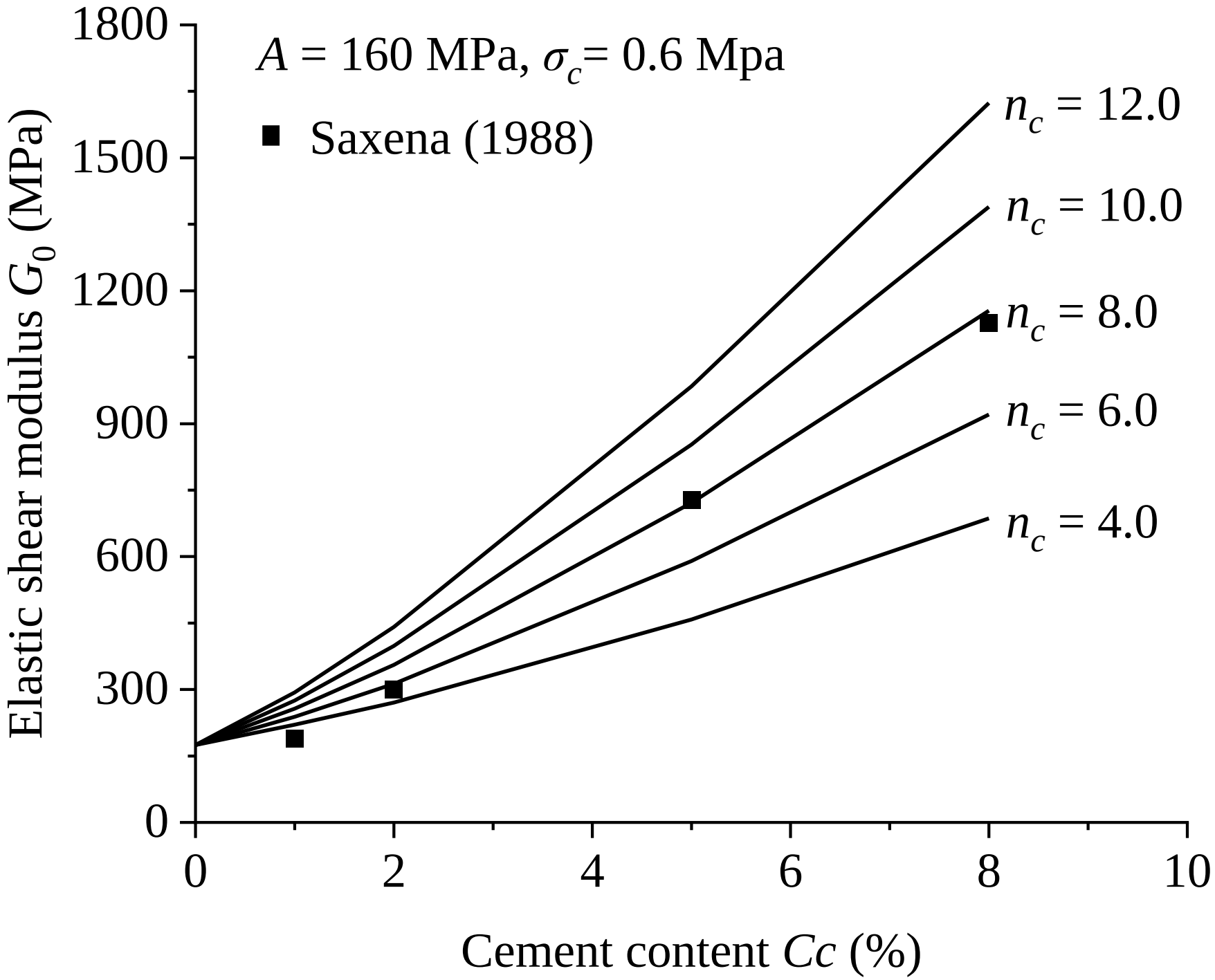

Fig. 4

Click here to access/download;Figure;Figure 4.pdf

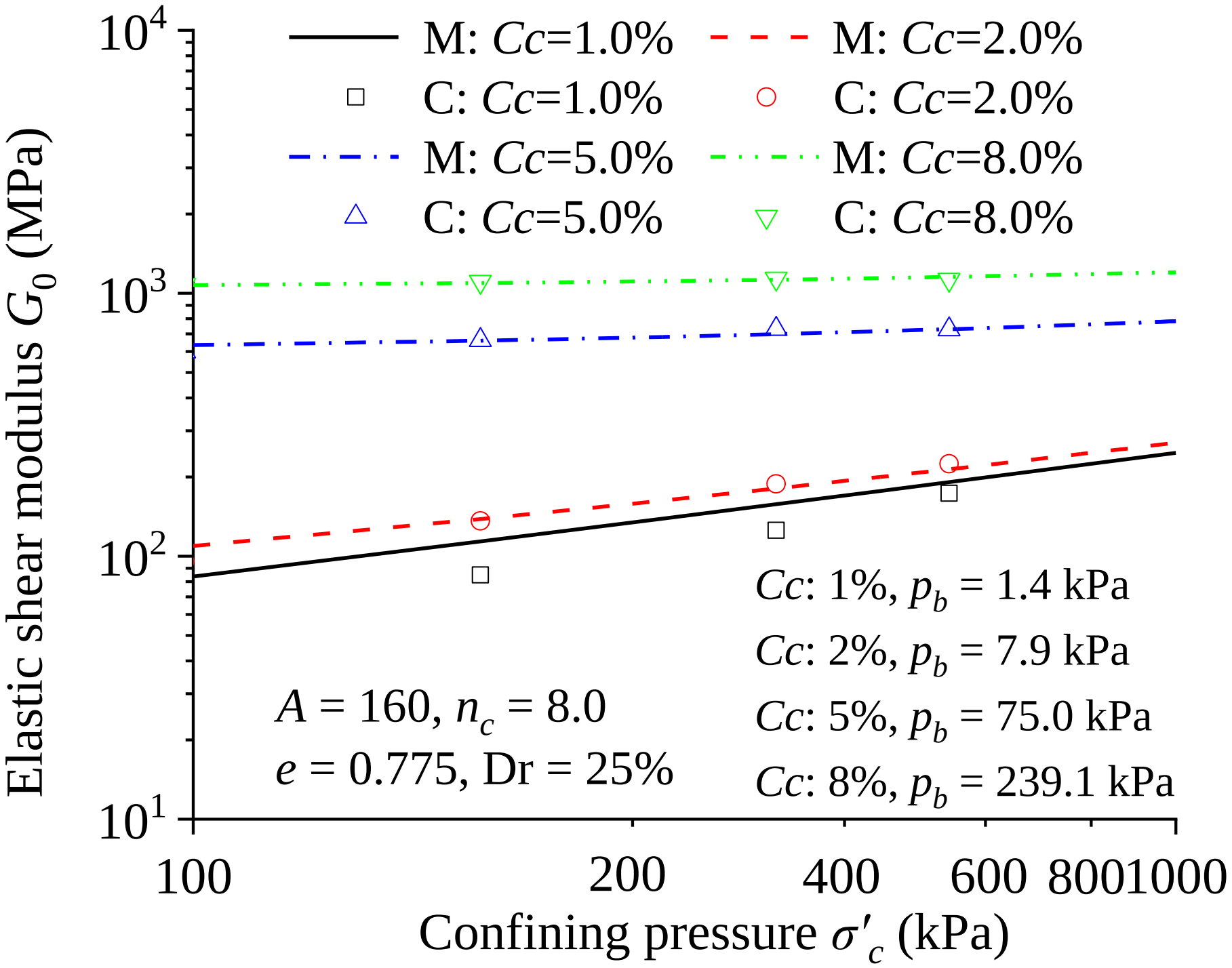

Fig. 5

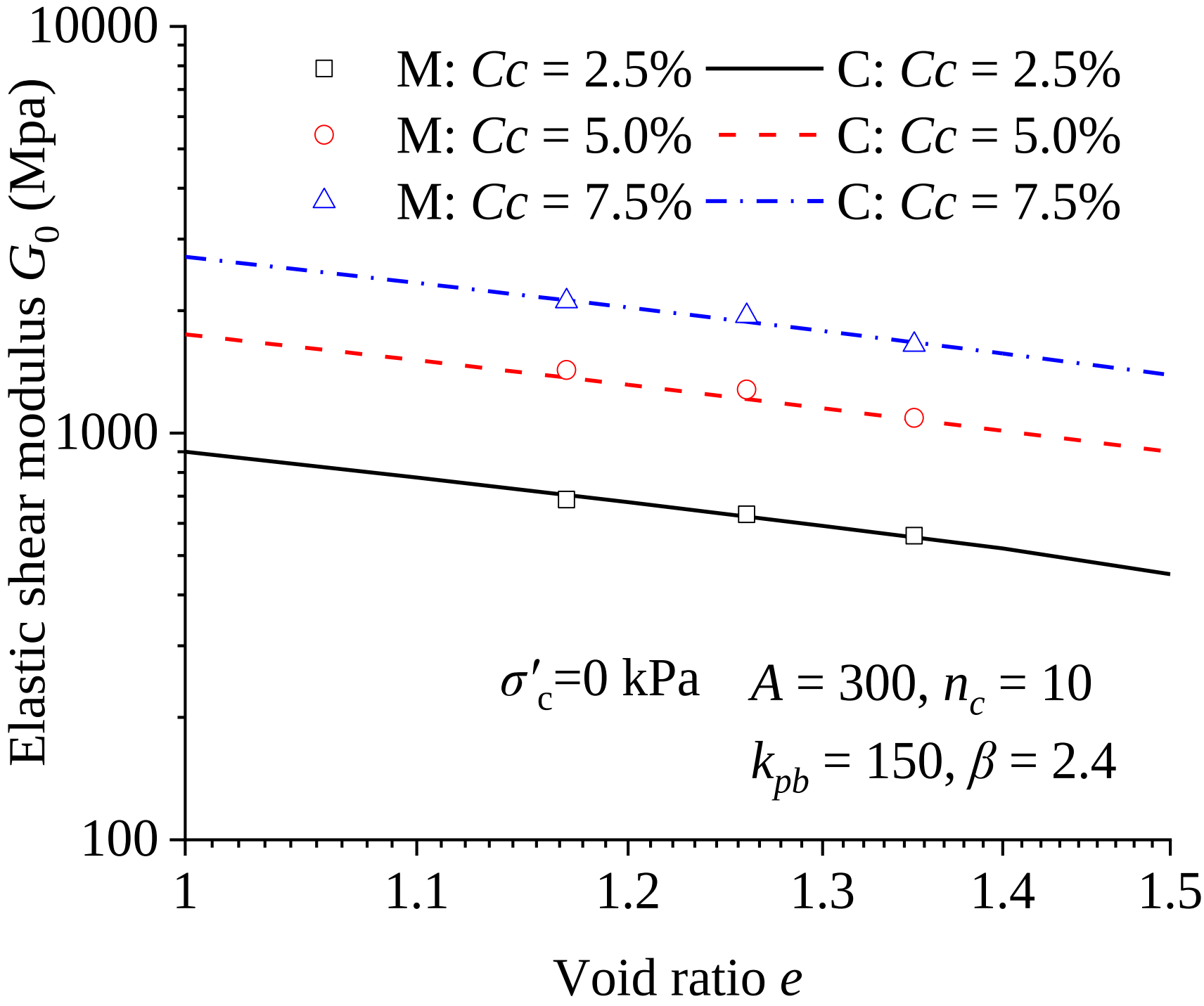

Fig. 6

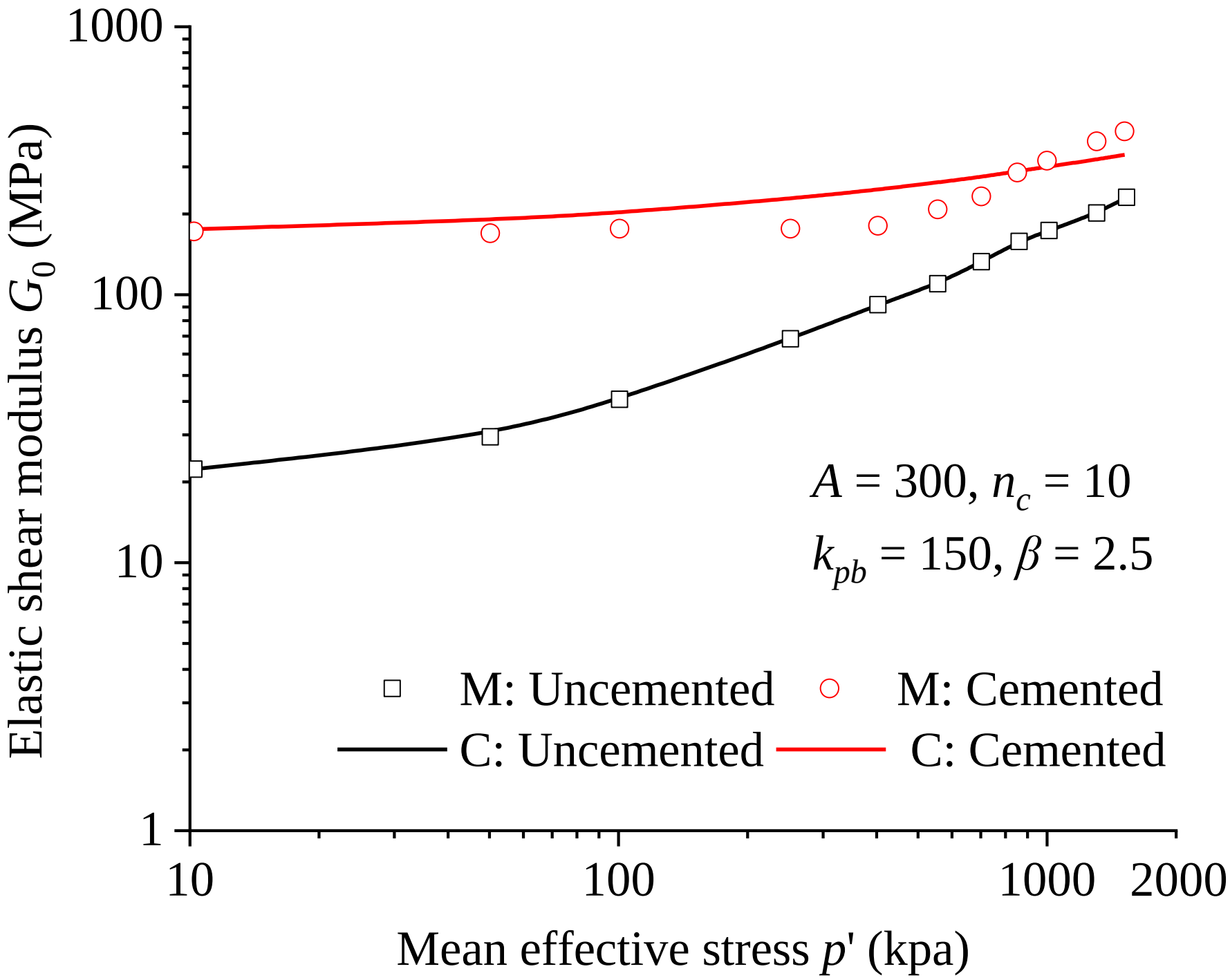

Fig. 7a1

Click here to access/download;Figure;Figure 7a-1.pdf

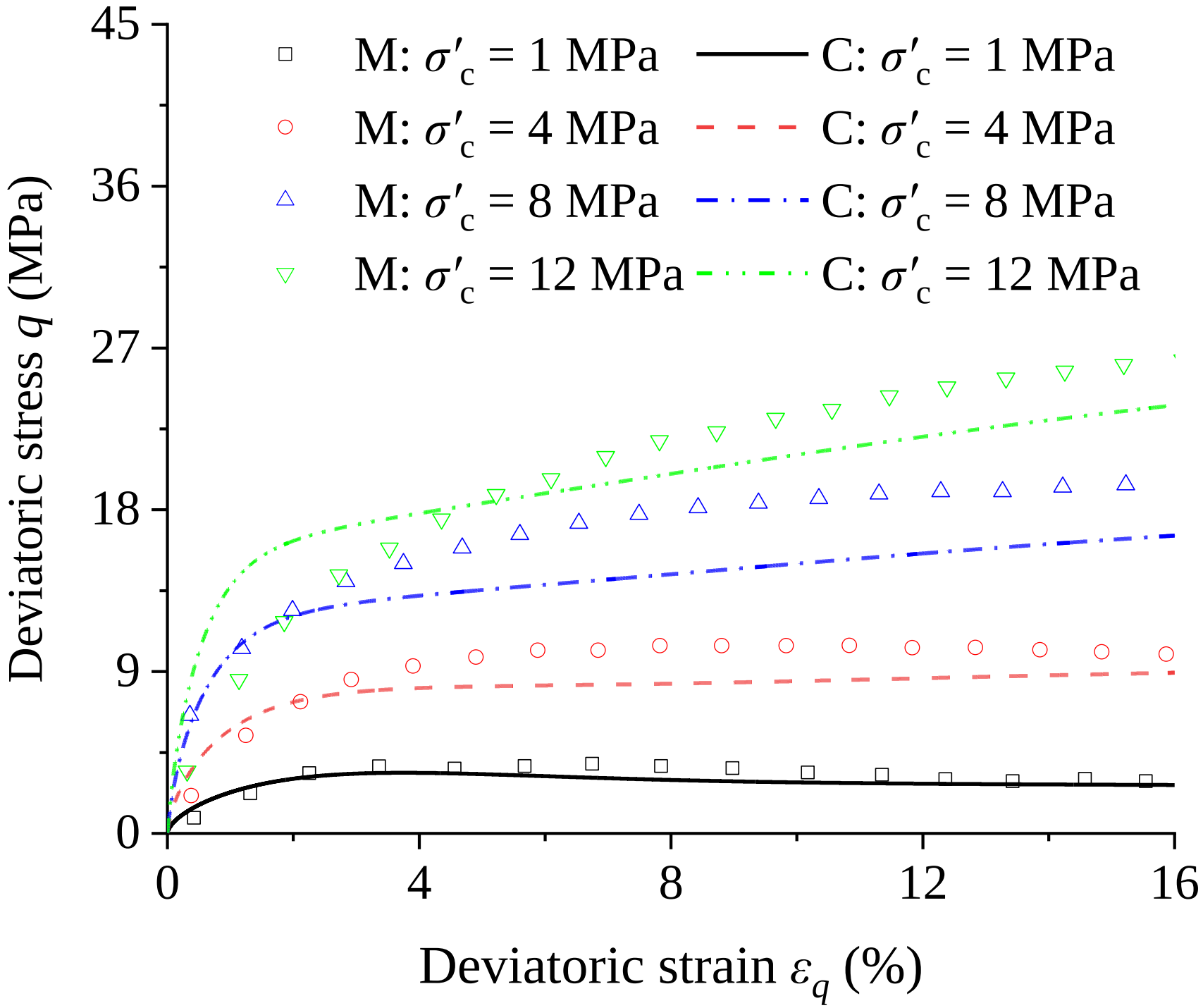

Fig. 7a2

Click here to access/download;Figure;Figure 7a-2.pdf

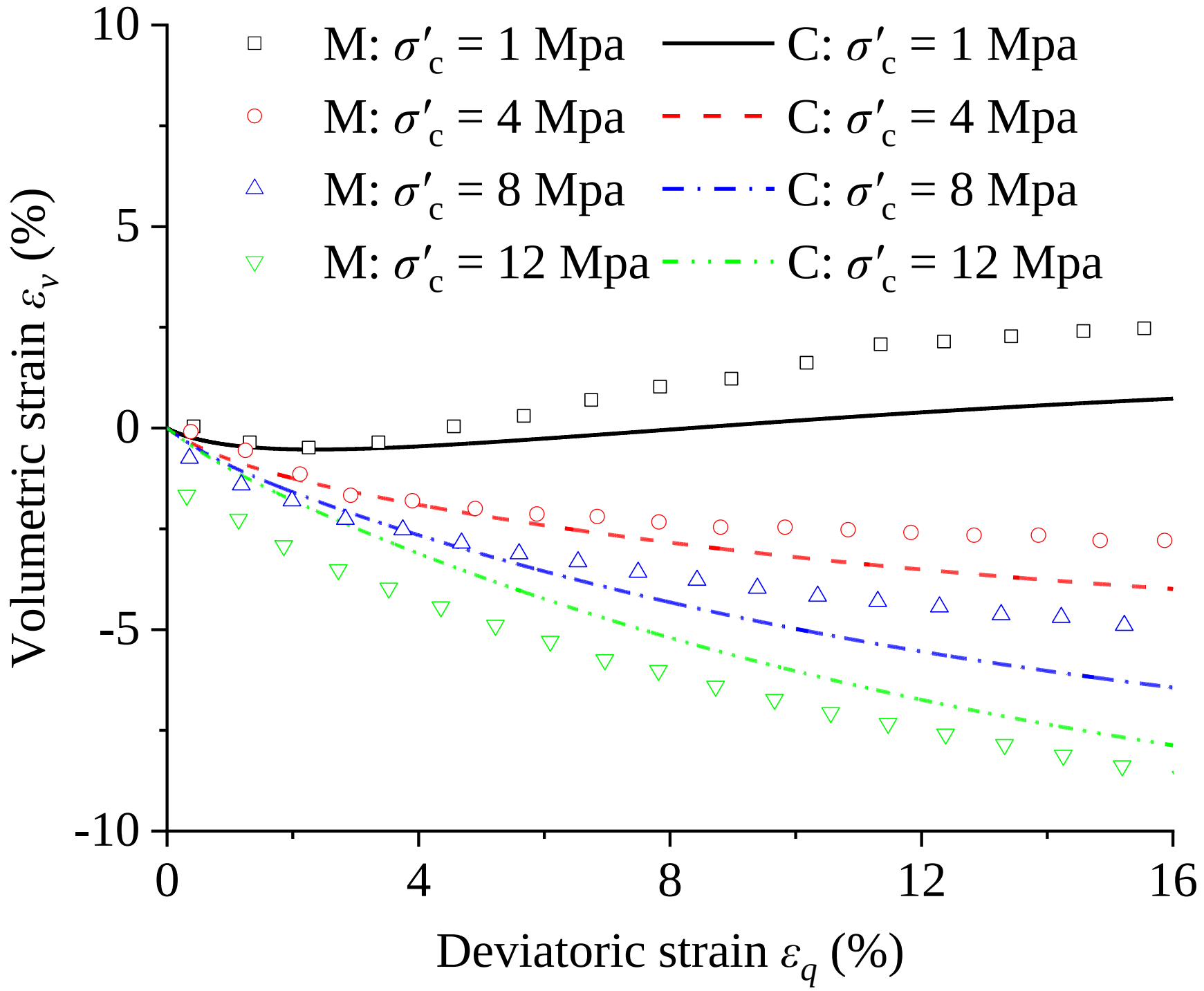

Fig. 7b1

Click here to access/download;Figure;Figure 7b-1.pdf

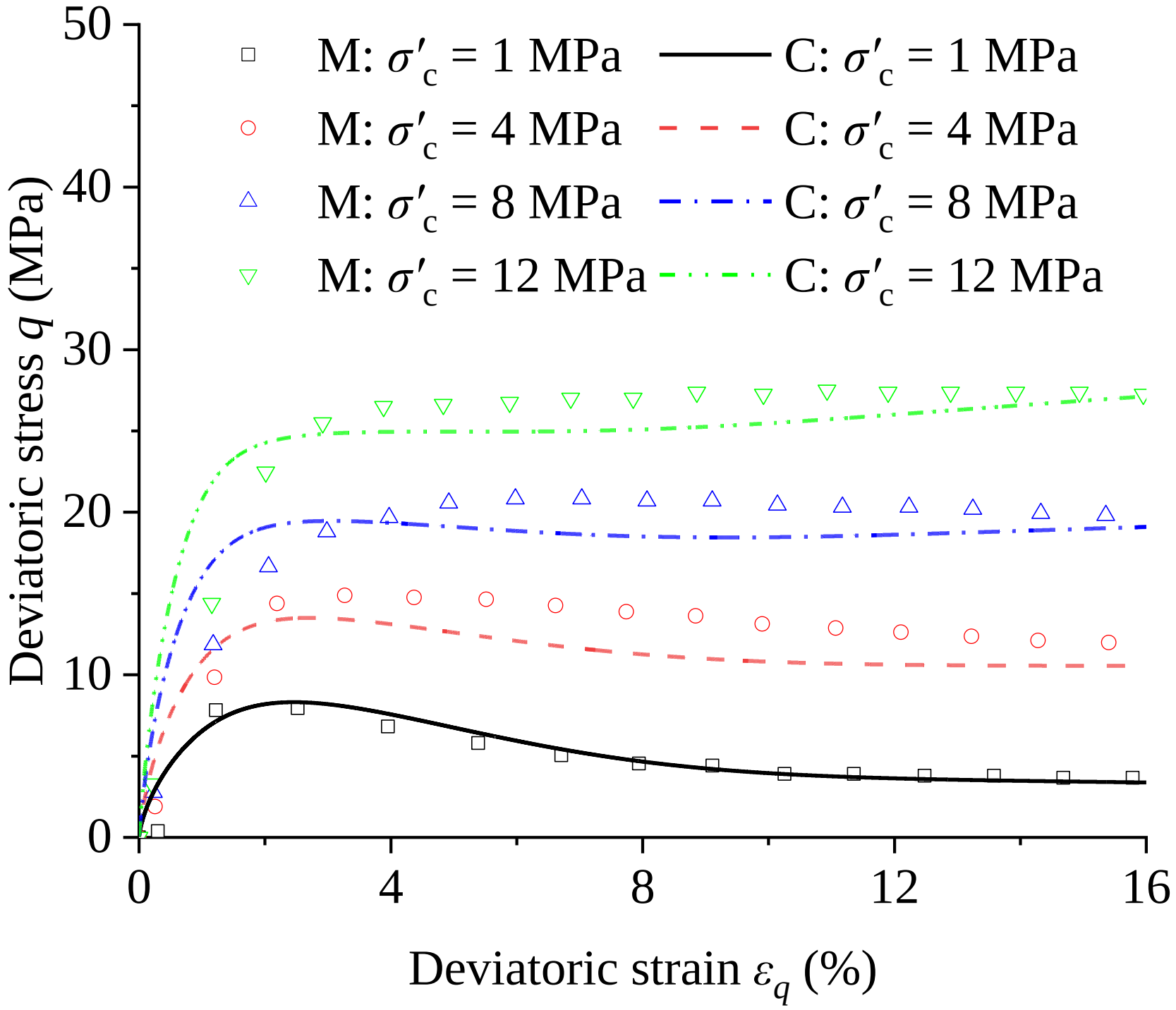

Fig. 7b2

Click here to access/download;Figure;Figure 7b-2.pdf

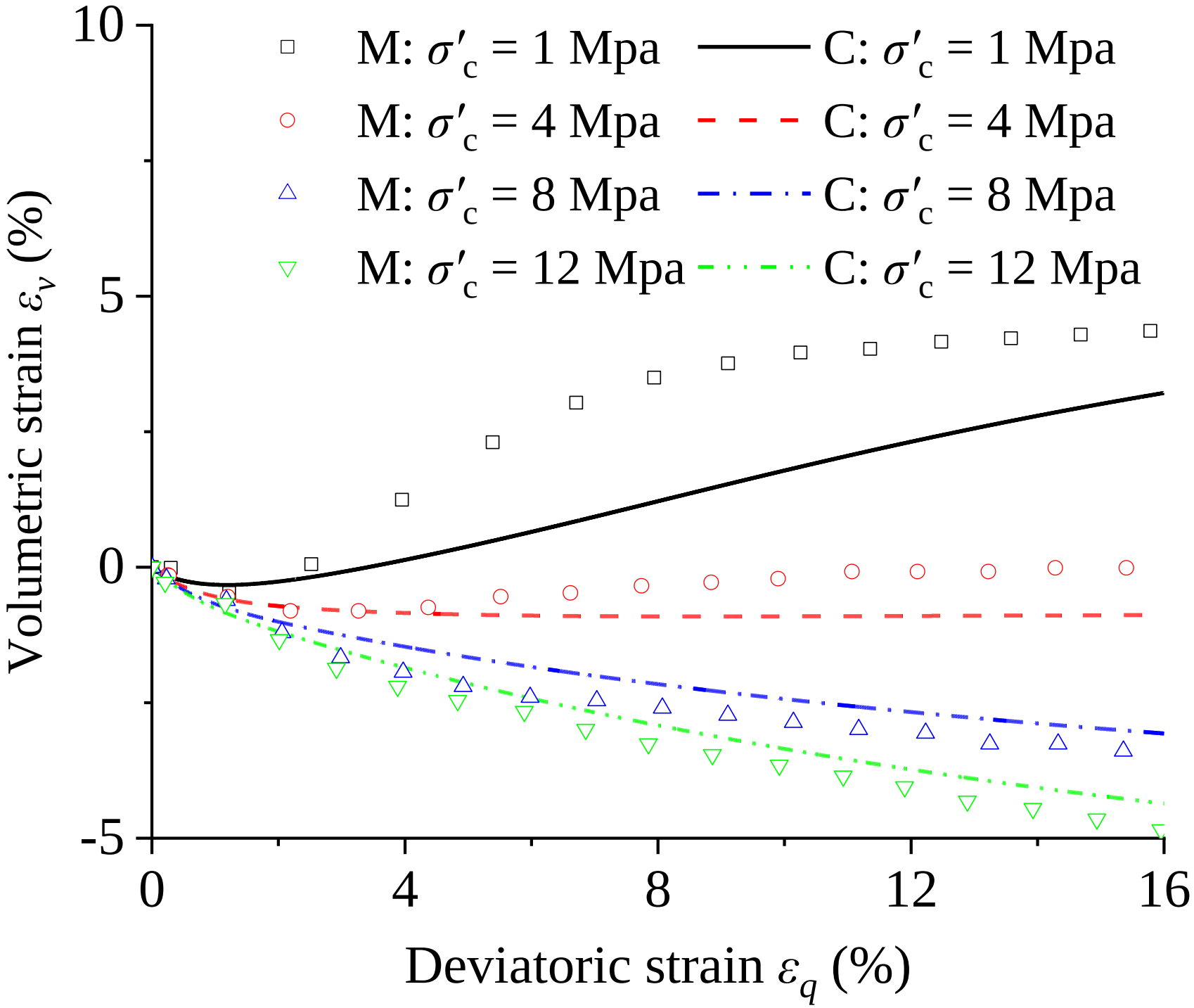

Fig. 7c1

Click here to access/download;Figure;Figure 7c-1.pdf

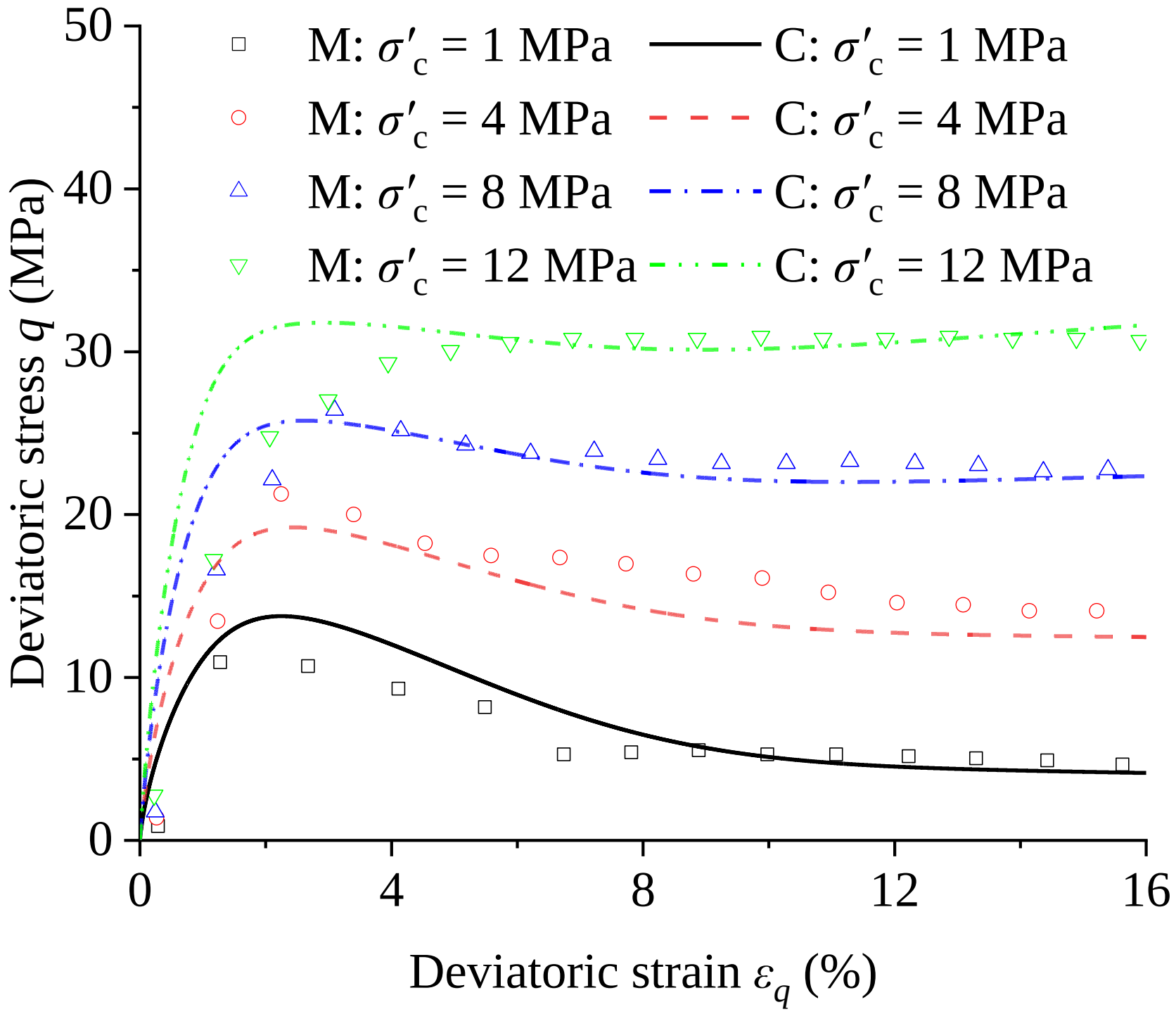

Fig. 7c2

Click here to access/download;Figure;Figure 7c-2.pdf

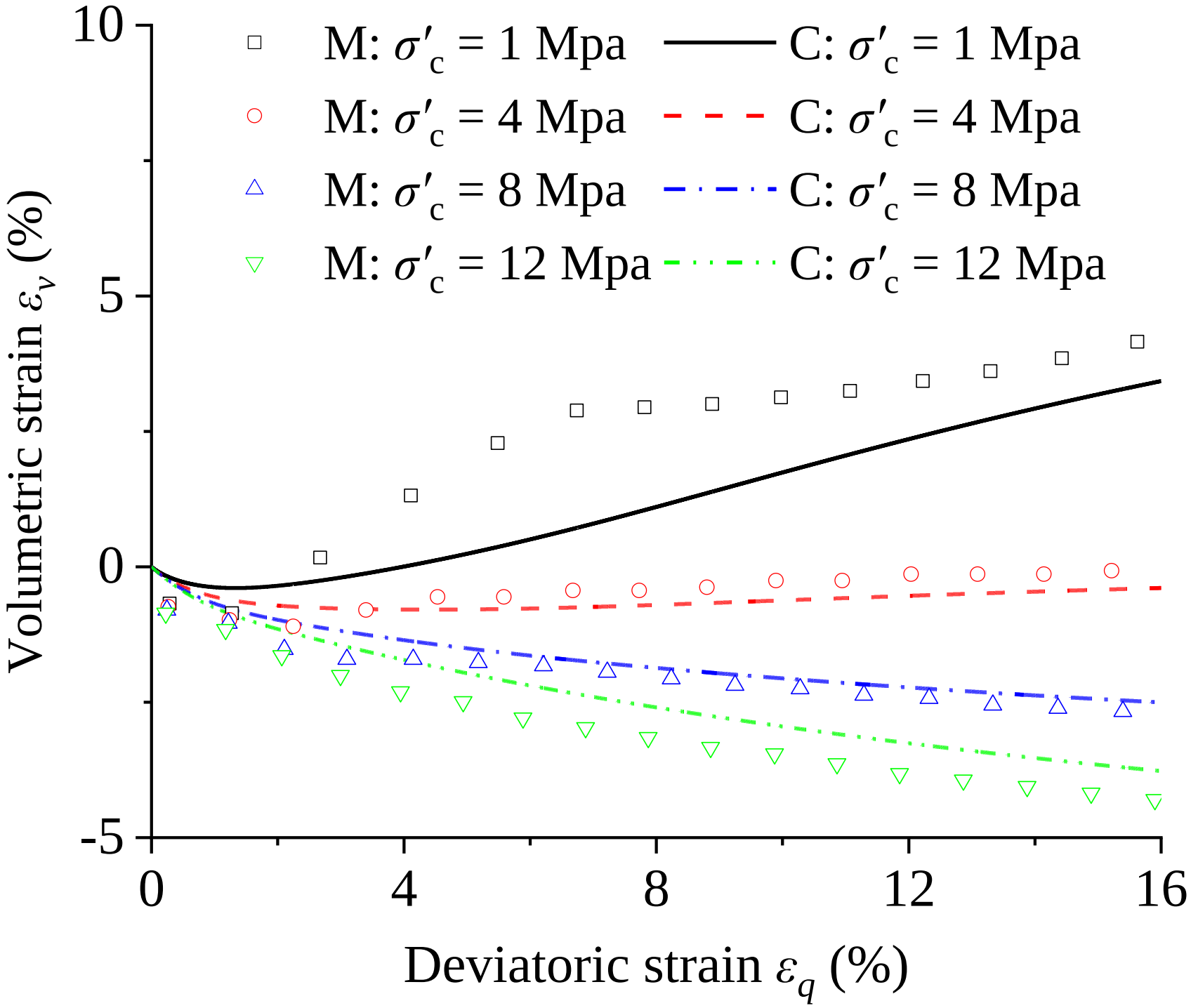

Fig. 8a1

Click here to access/download;Figure;Figure 8a-1.pdf

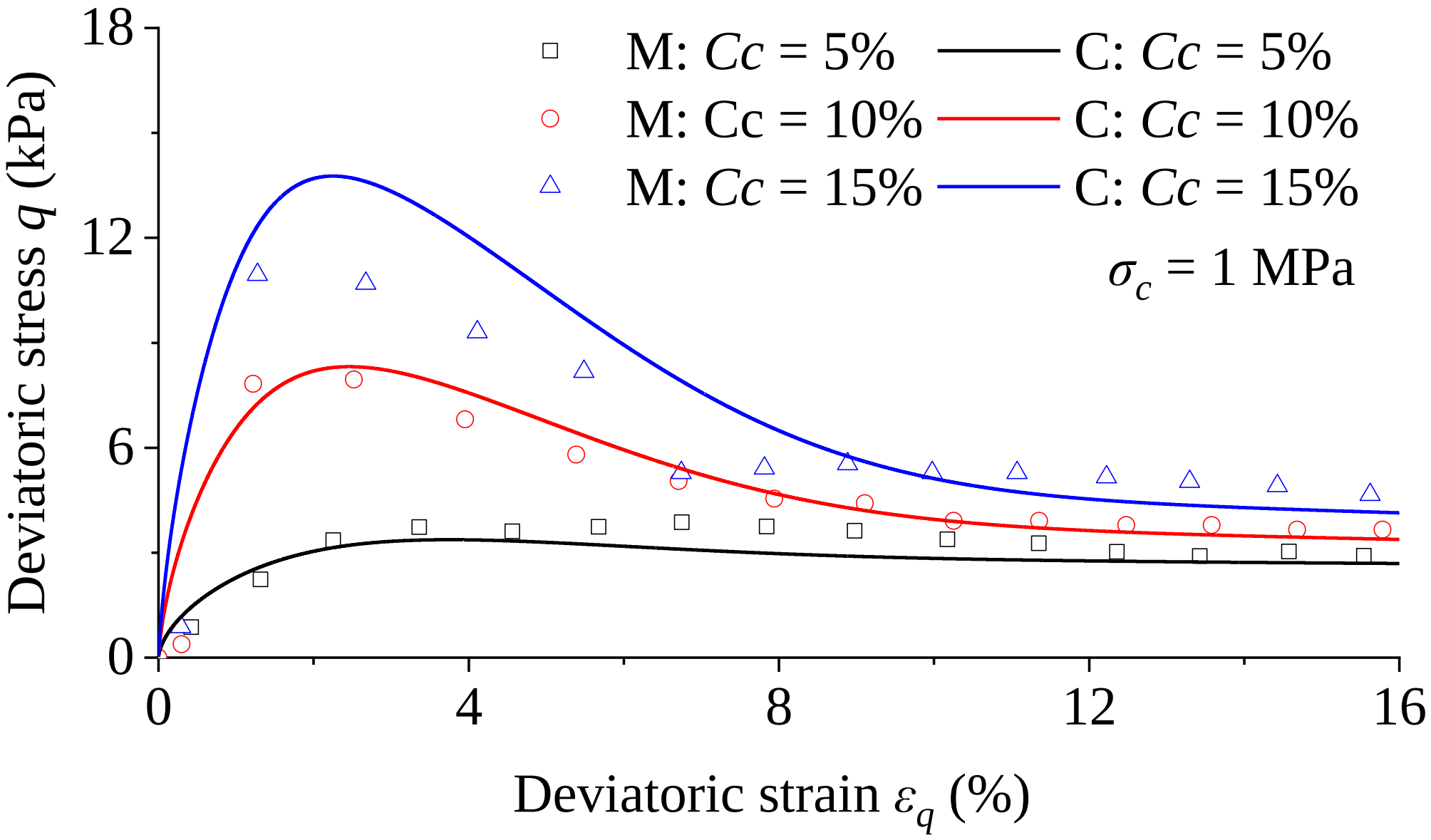

Fig. 8a2

Click here to access/download;Figure;Figure 8a-2.pdf

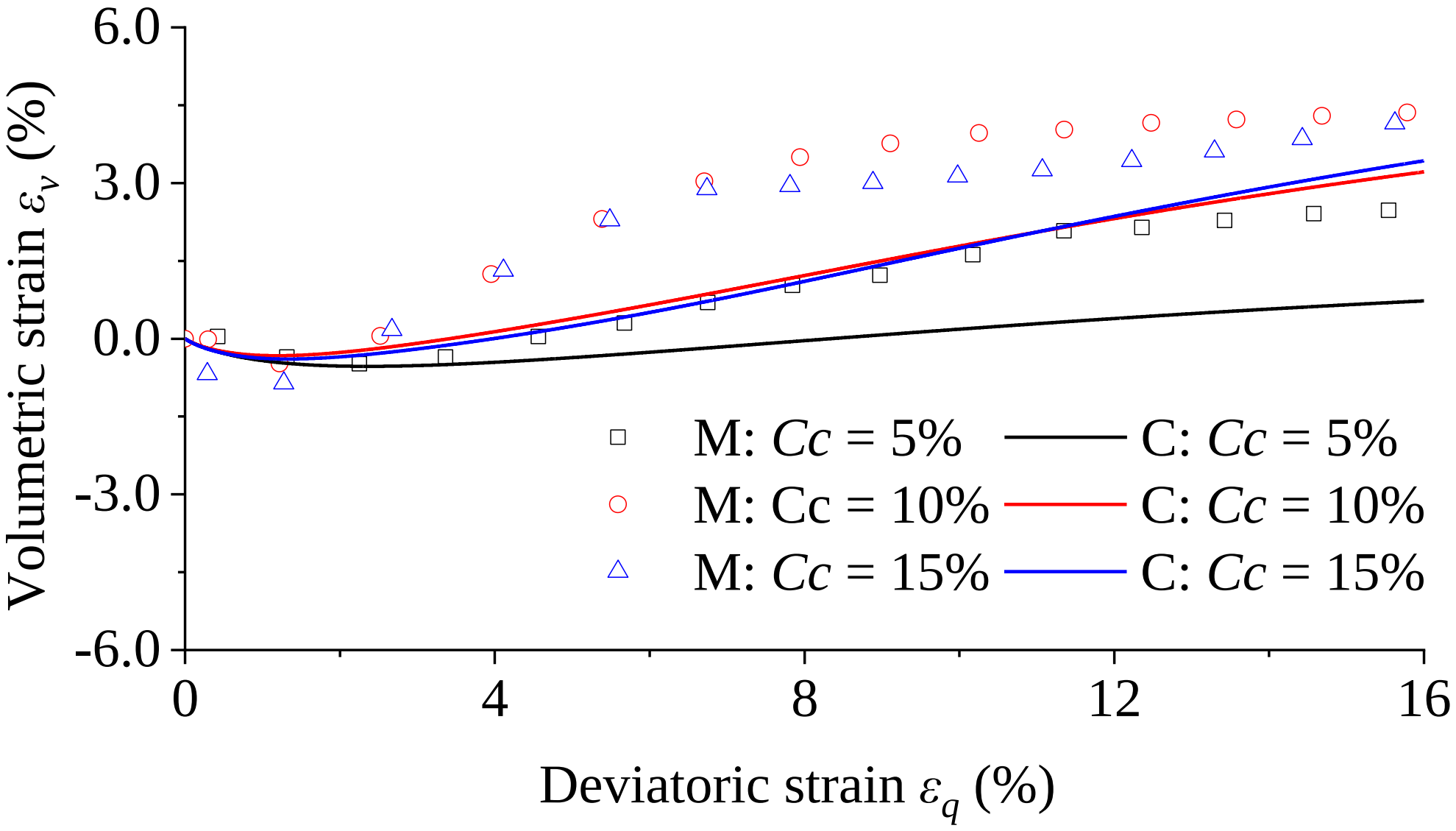

Fig. 8b1

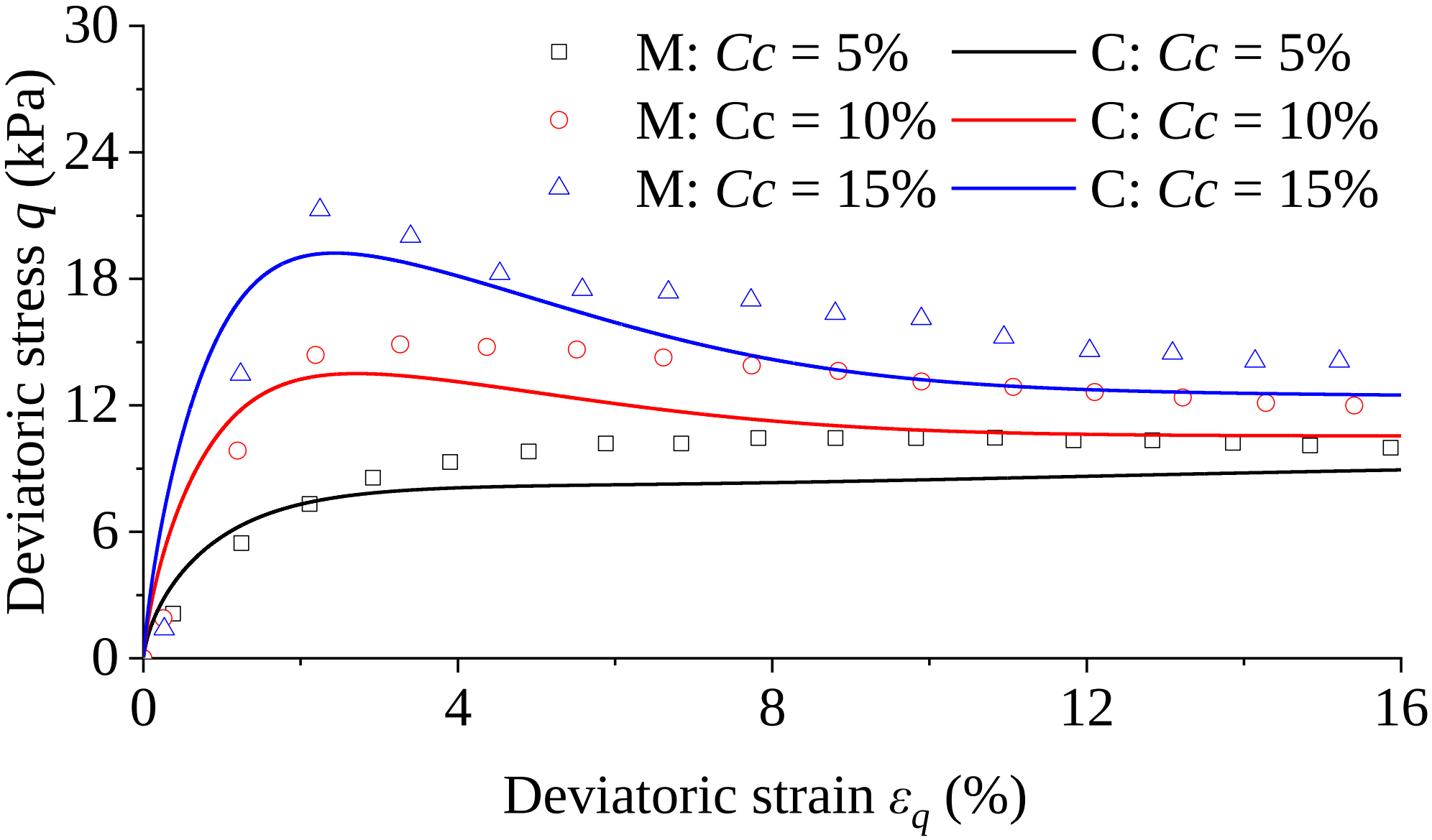

Fig. 8b2

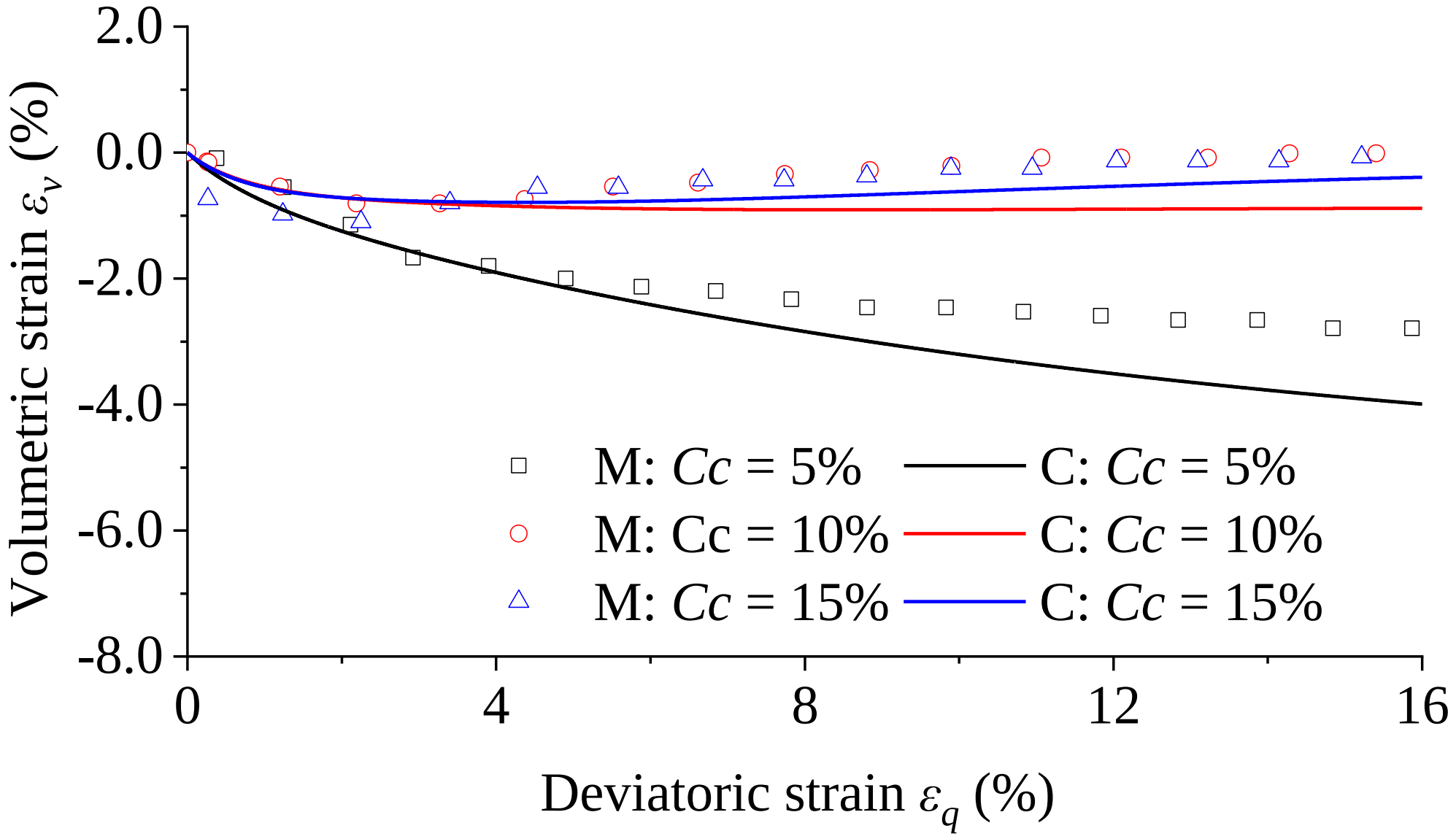

Fig. 8c1

Click here to access/download;Figure;Figure 8c-1.pdf

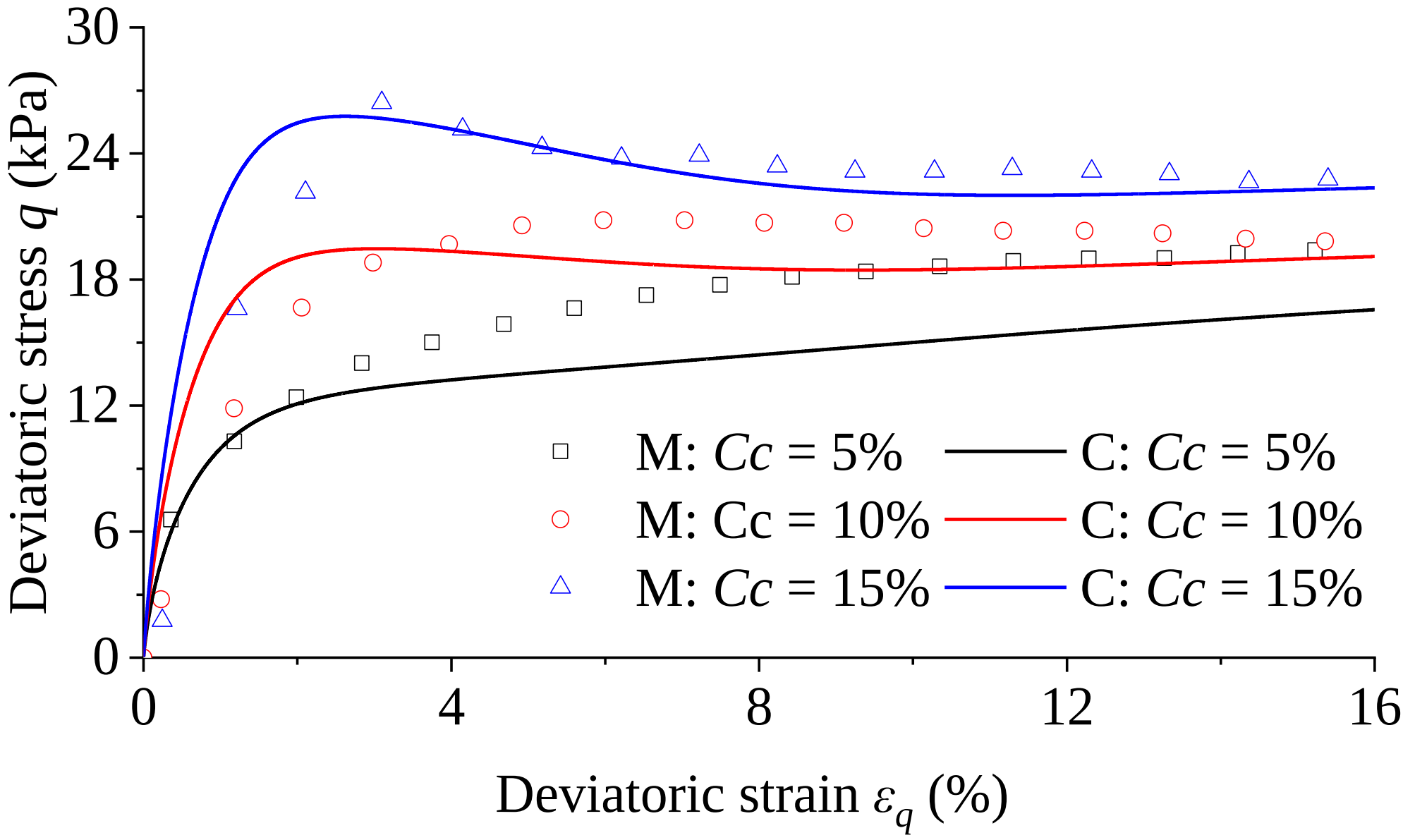

Fig. 8c2

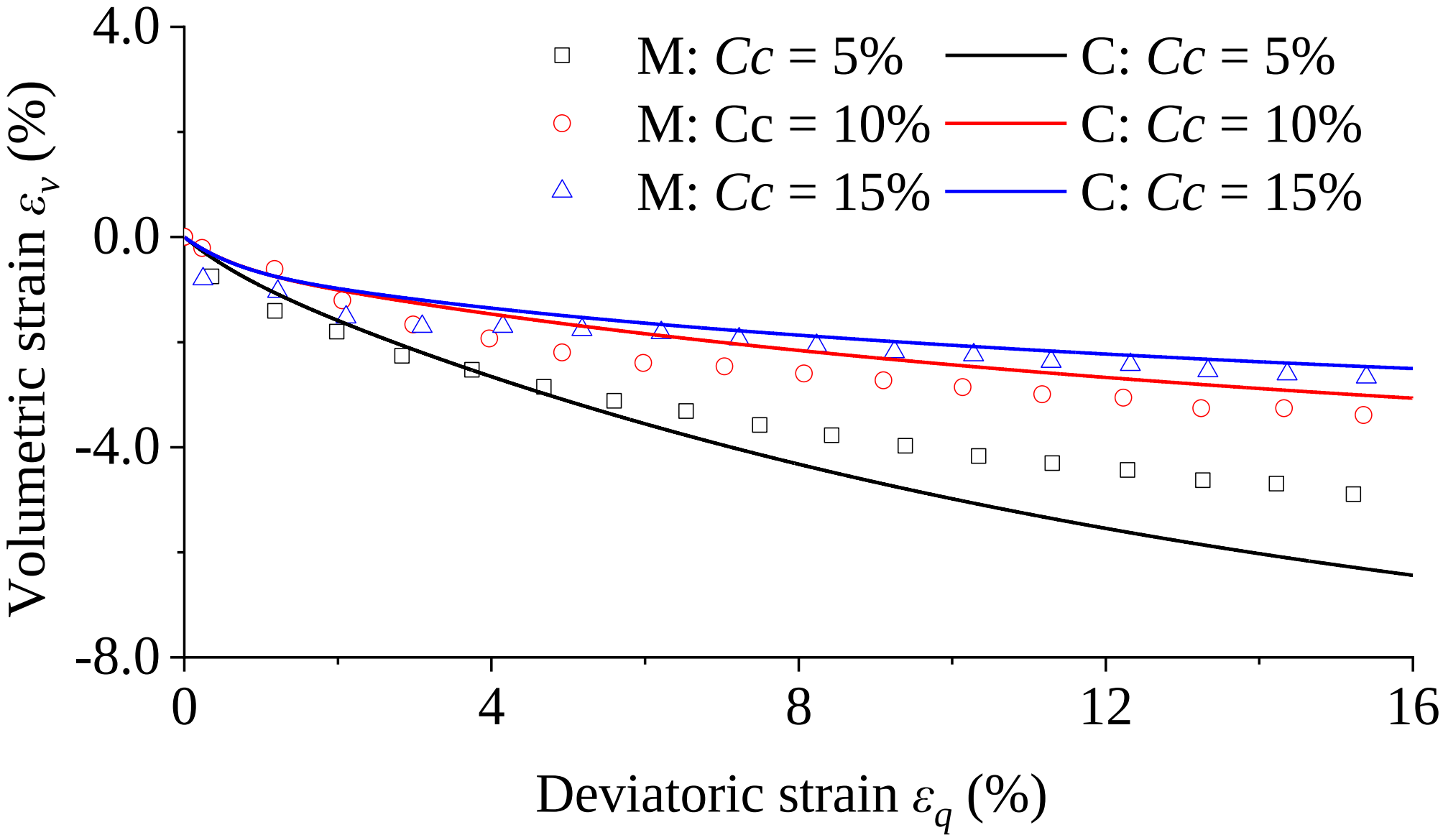

Fig. 8d1

Click here to access/download;Figure;Figure 8d-1.pdf

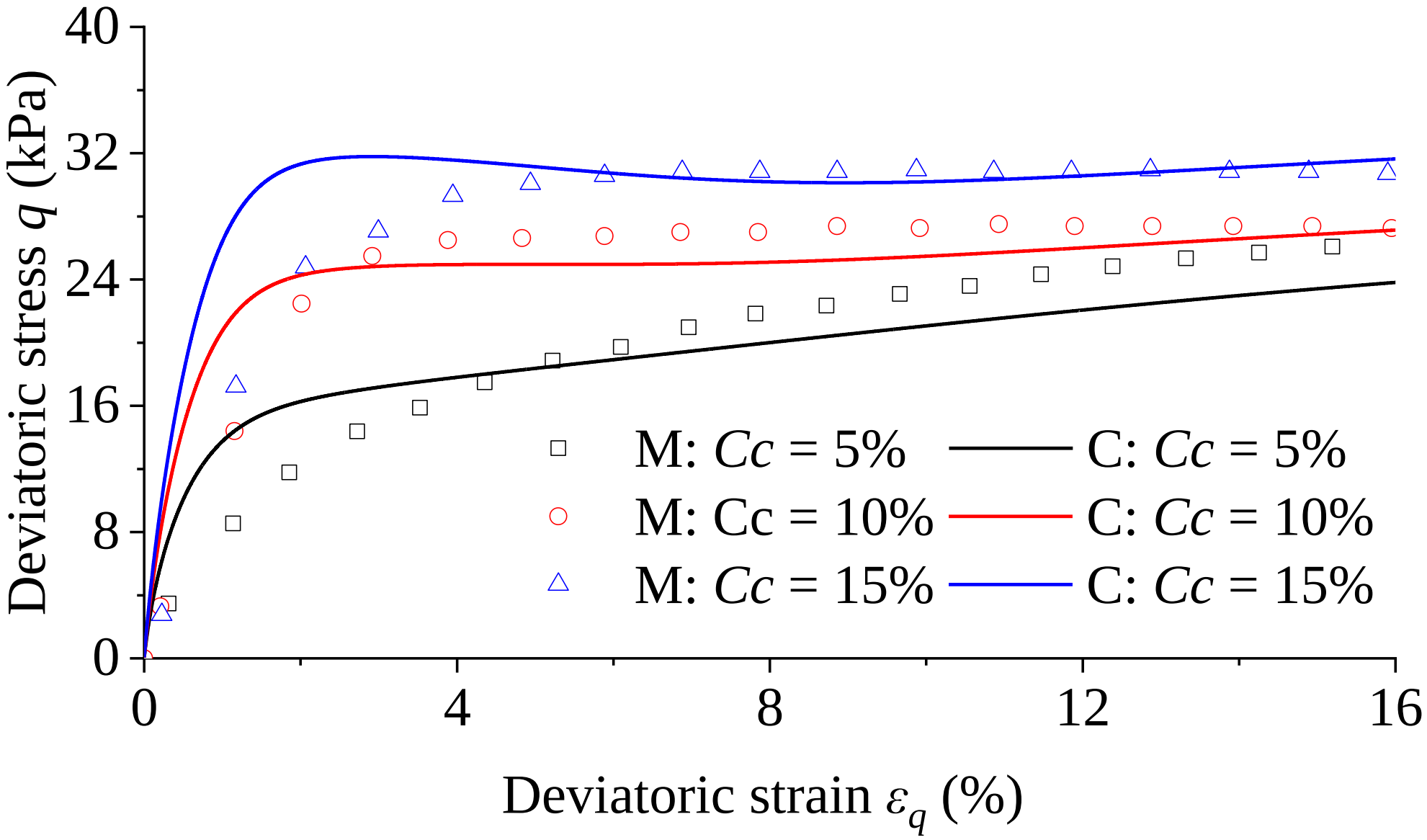

Fig. 8d2

Click here to access/download;Figure;Figure 8d-2.pdf

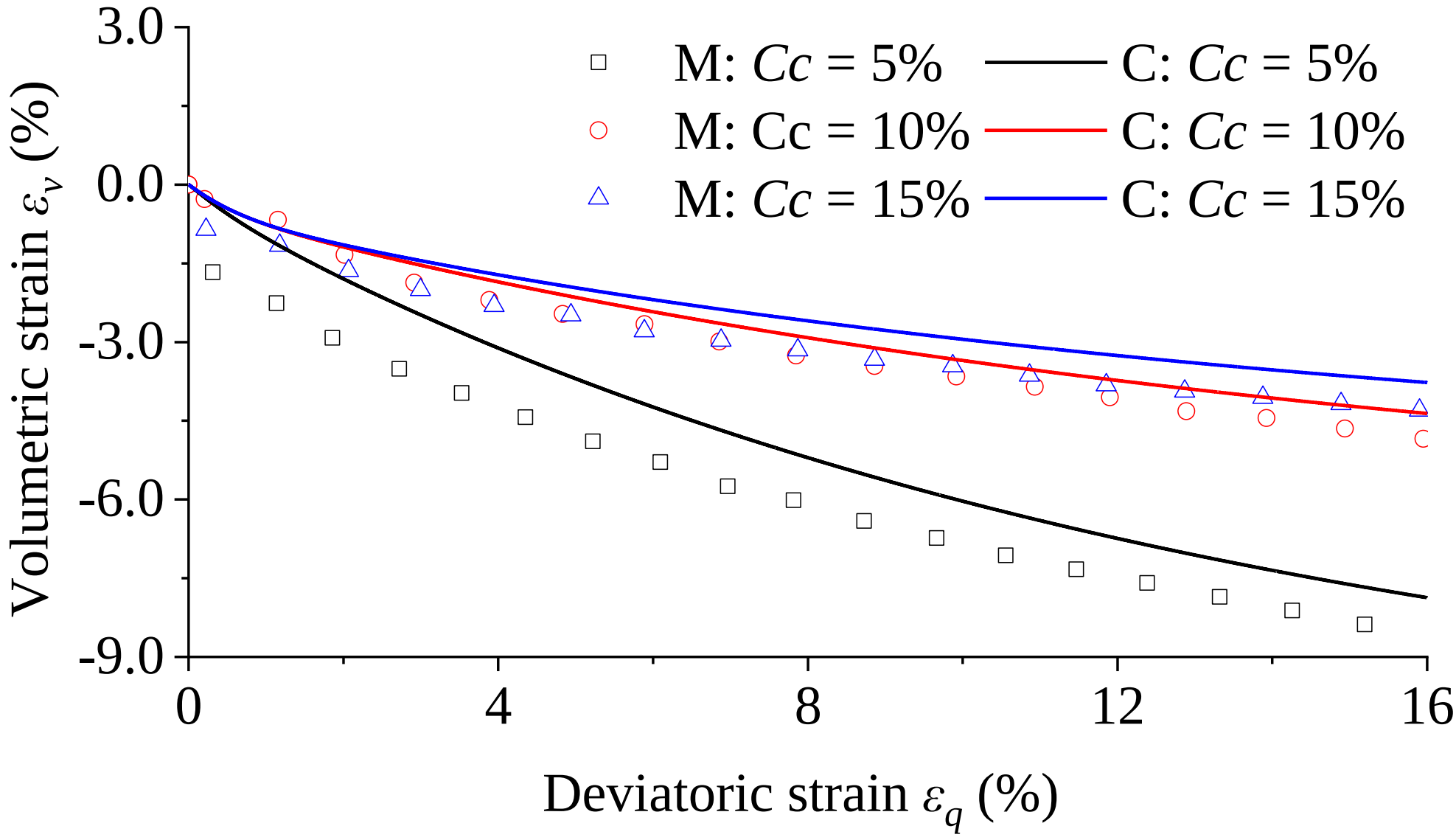

Fig. 9a1

Click here to access/download;Figure;Figure 9a-1.pdf

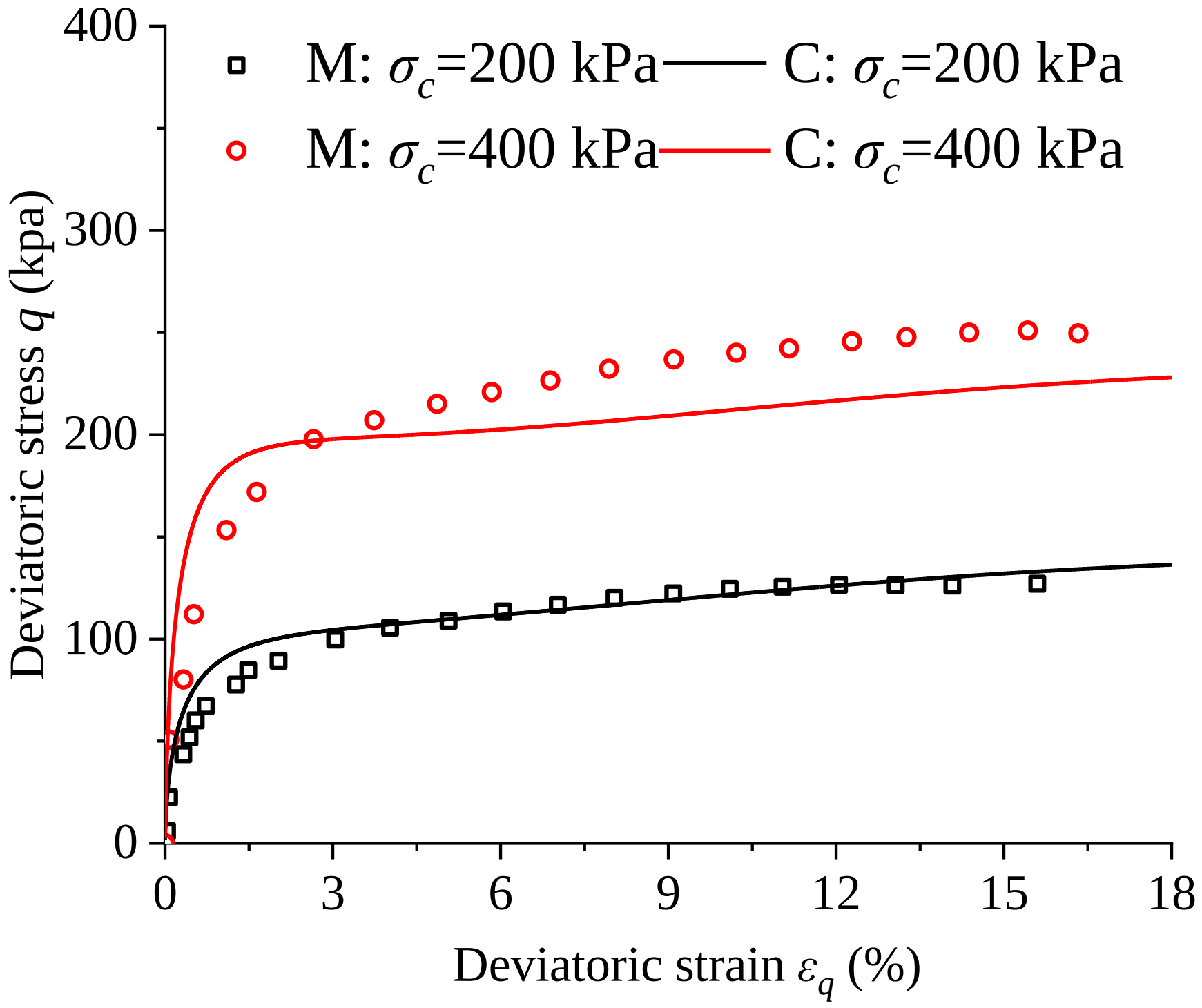

Fig. 9a2

Click here to access/download;Figure;Figure 9a-2.pdf

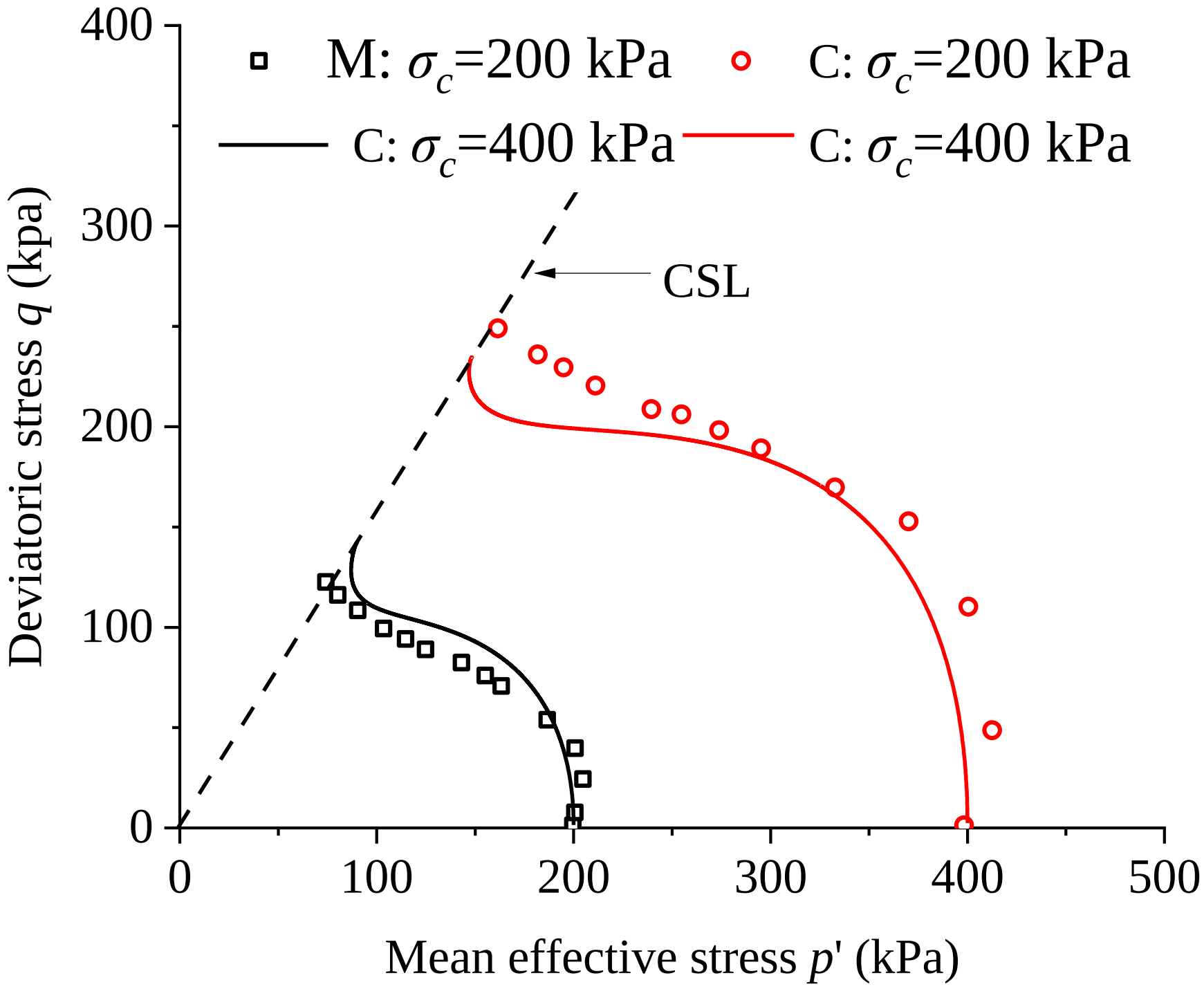

Fig. 9b1

Click here to access/download;Figure;Figure 9b-1.pdf

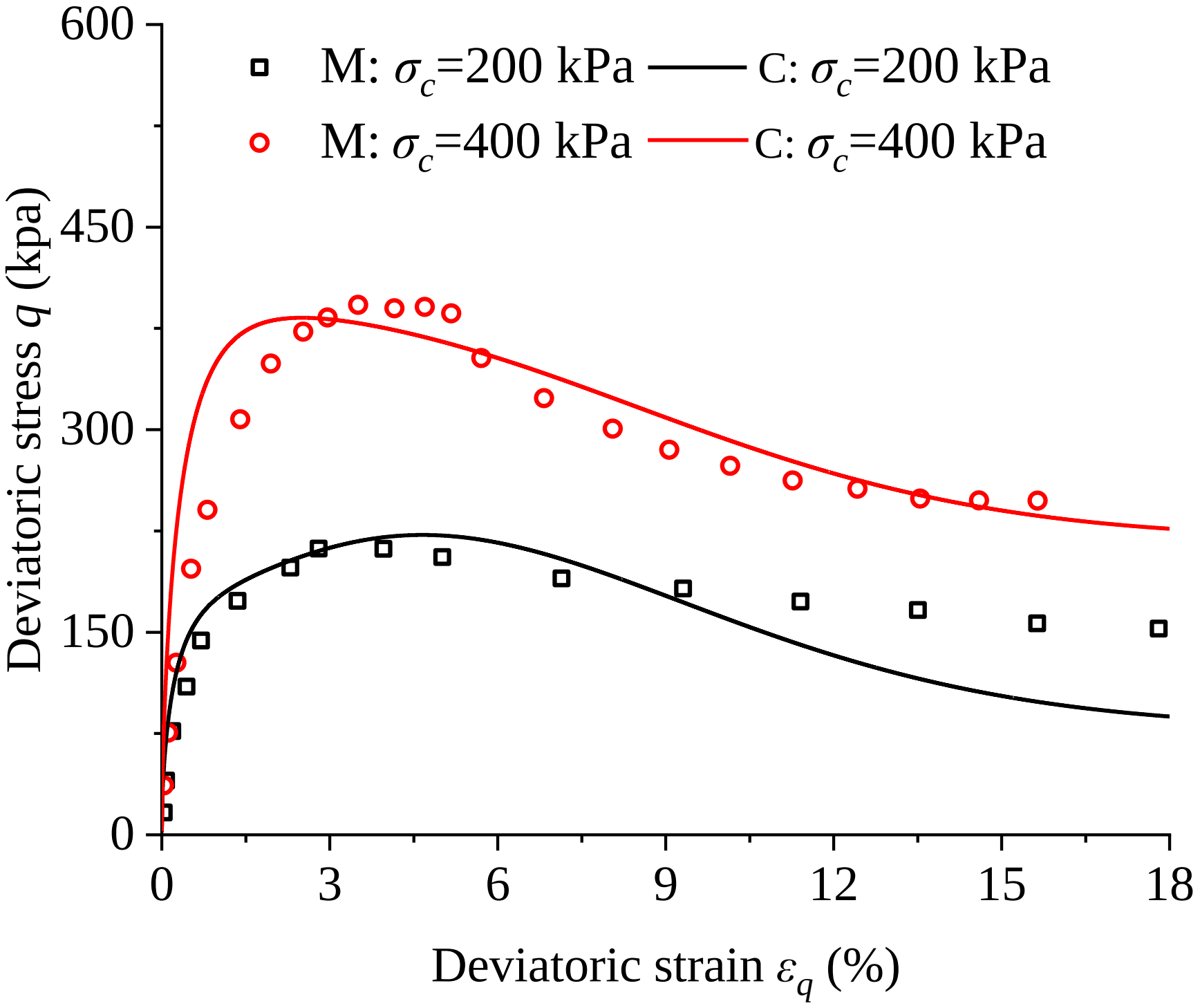

Fig. 9b2

Click here to access/download;Figure;Figure 9b-2.pdf

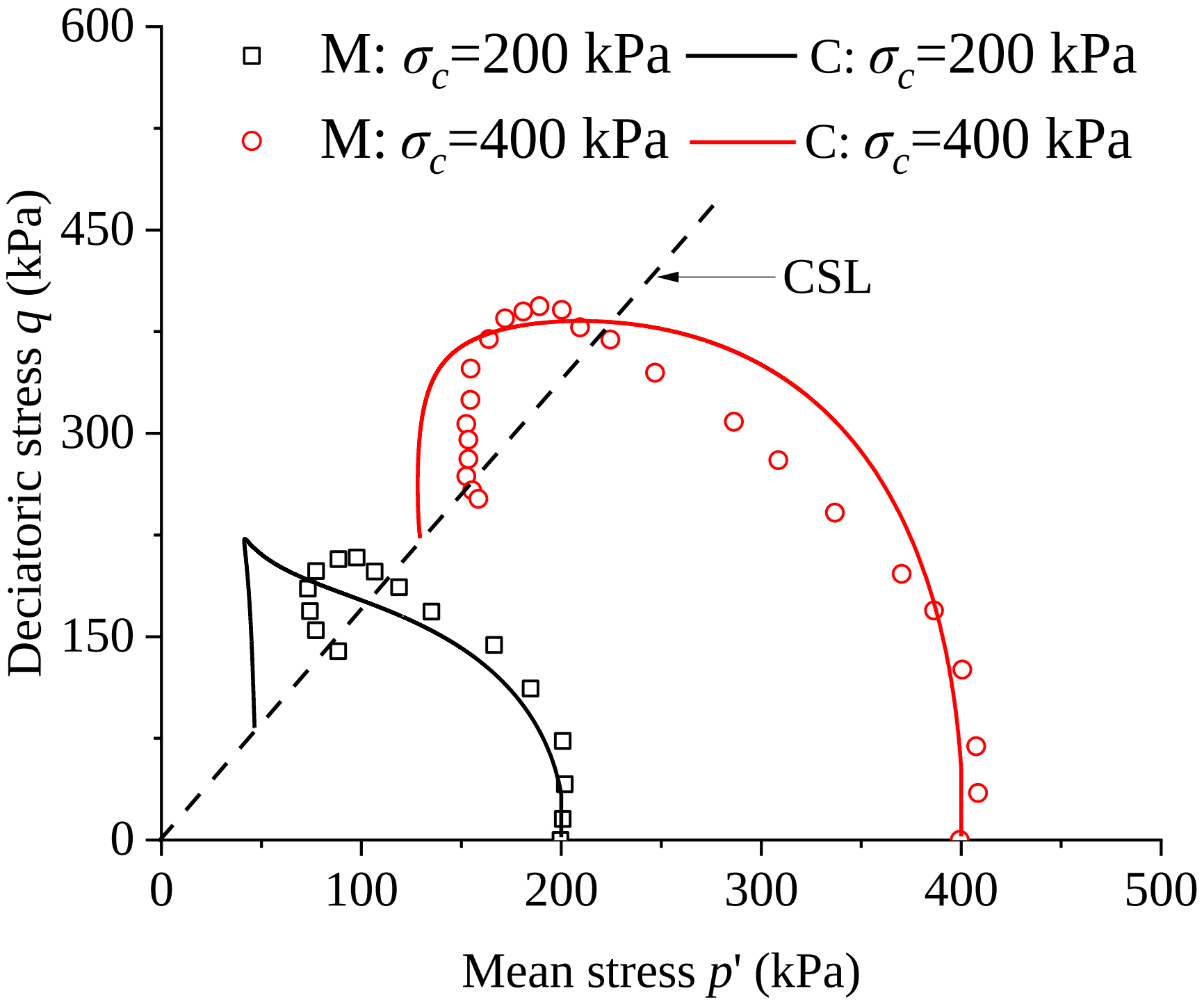

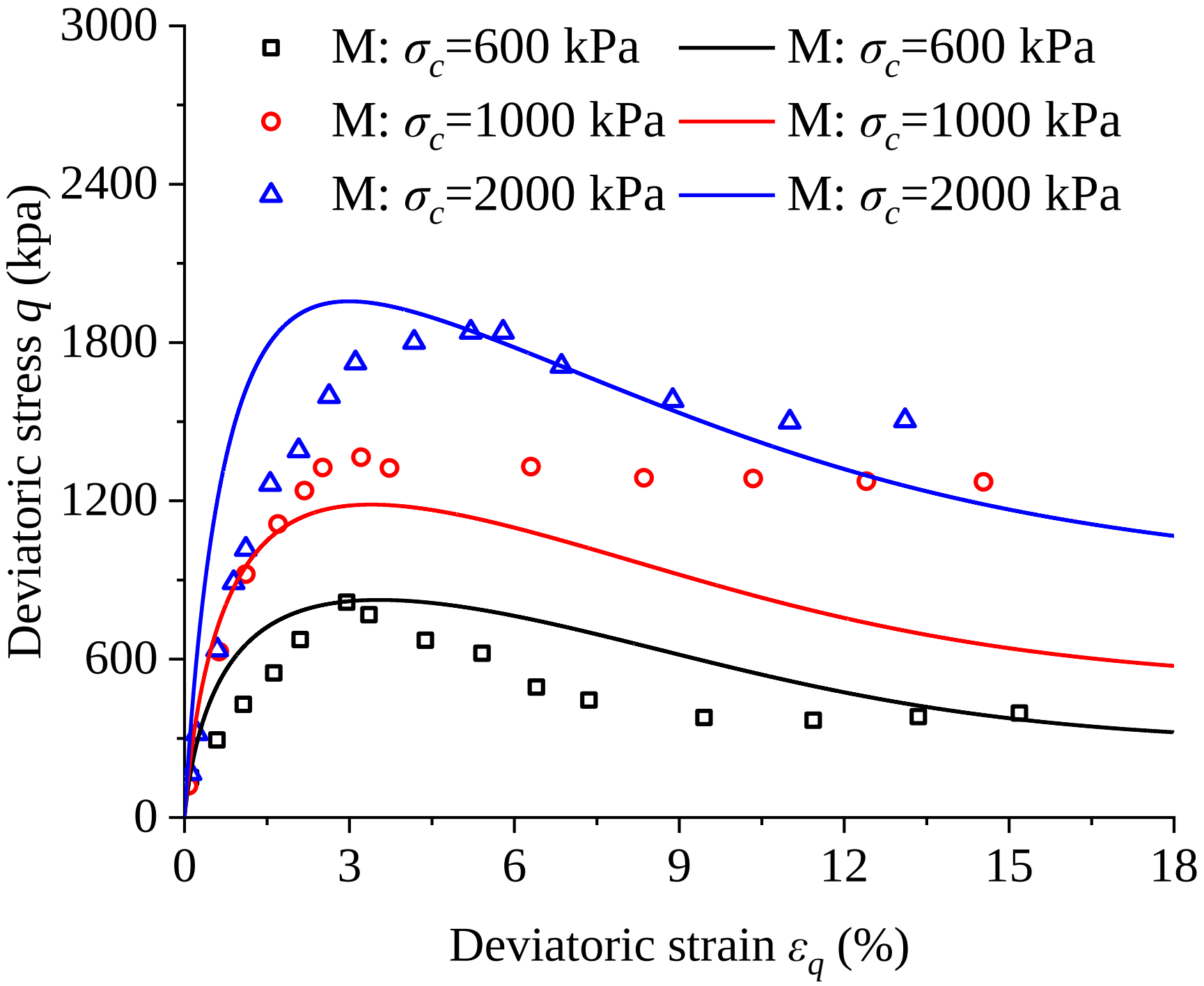

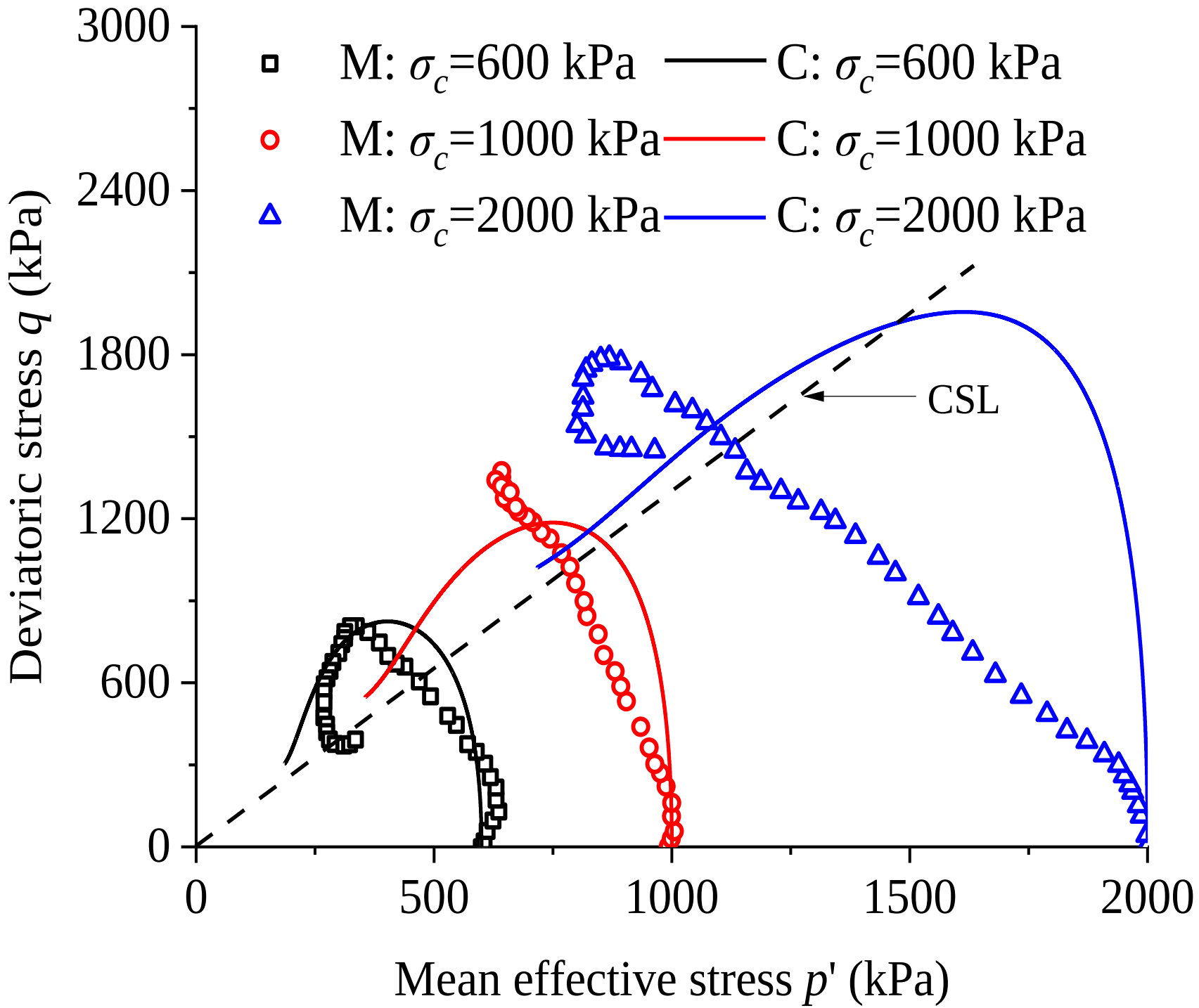

Fig. 10a

Click here to access/download;Figure;Figure 10a.pdf

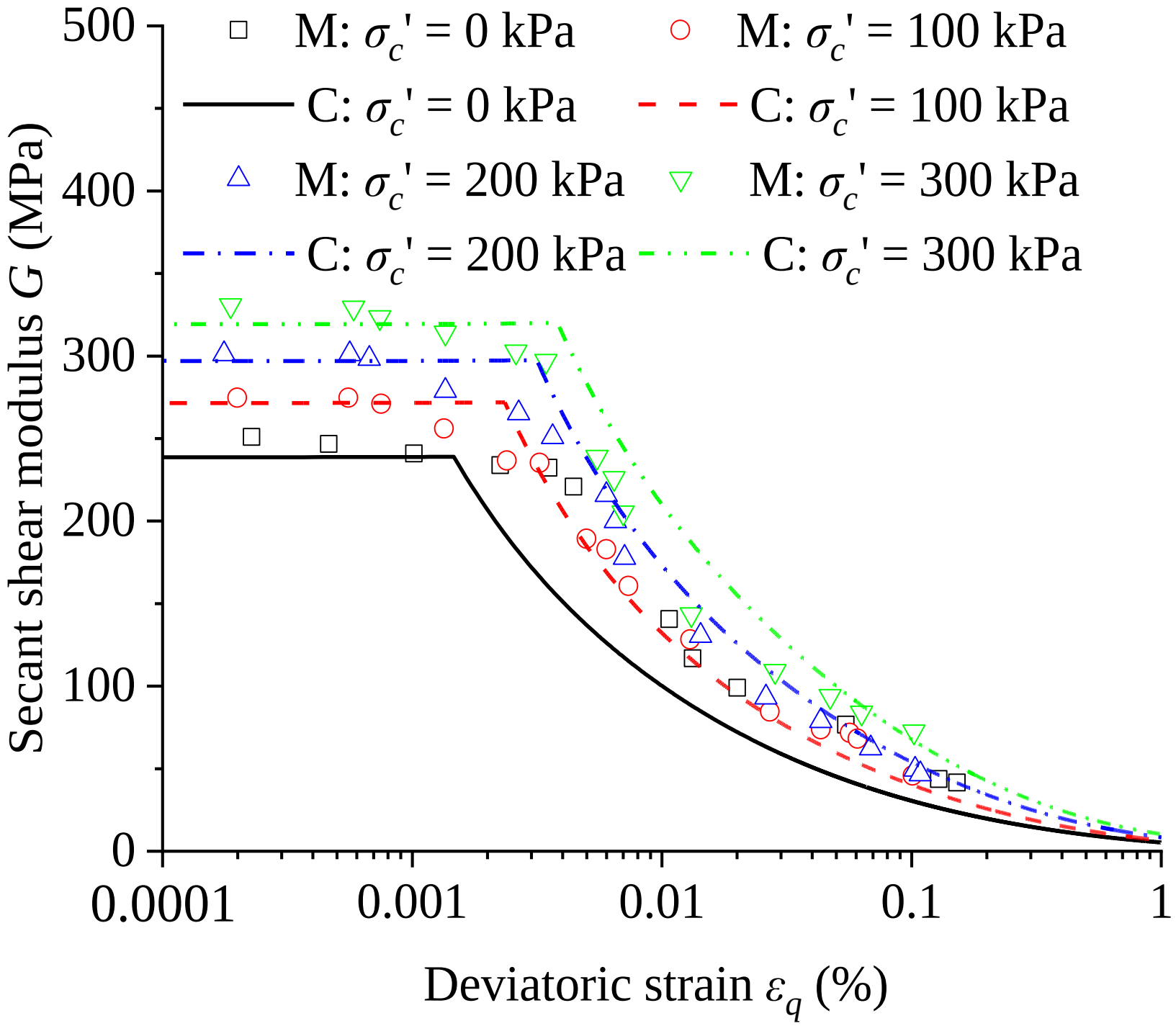

Fig. 10b

Click here to access/download;Figure;Figure 10b.pdf

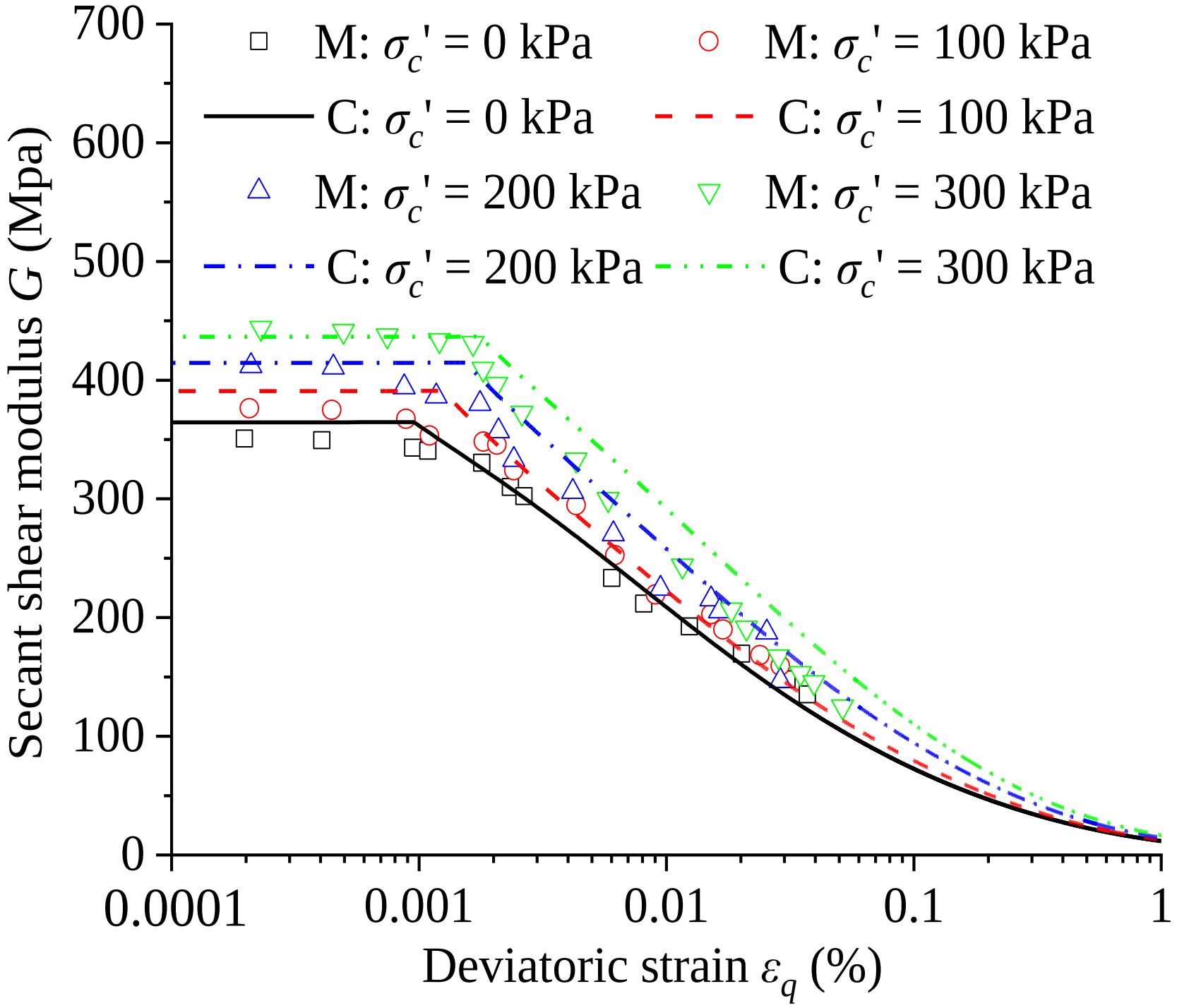

Fig. 10c

Click here to access/download;Figure;Figure 10c.pdf

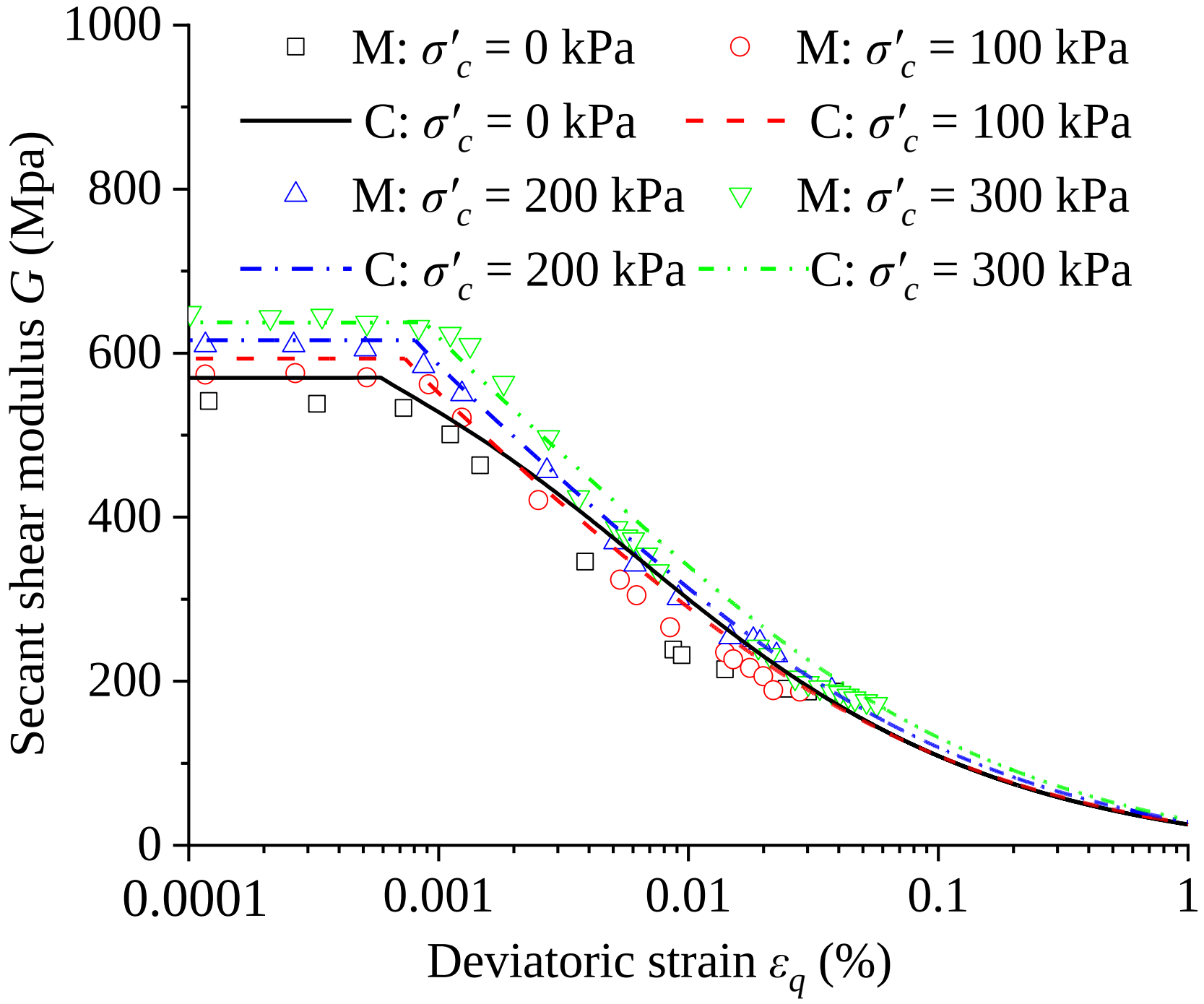

Fig. 11a

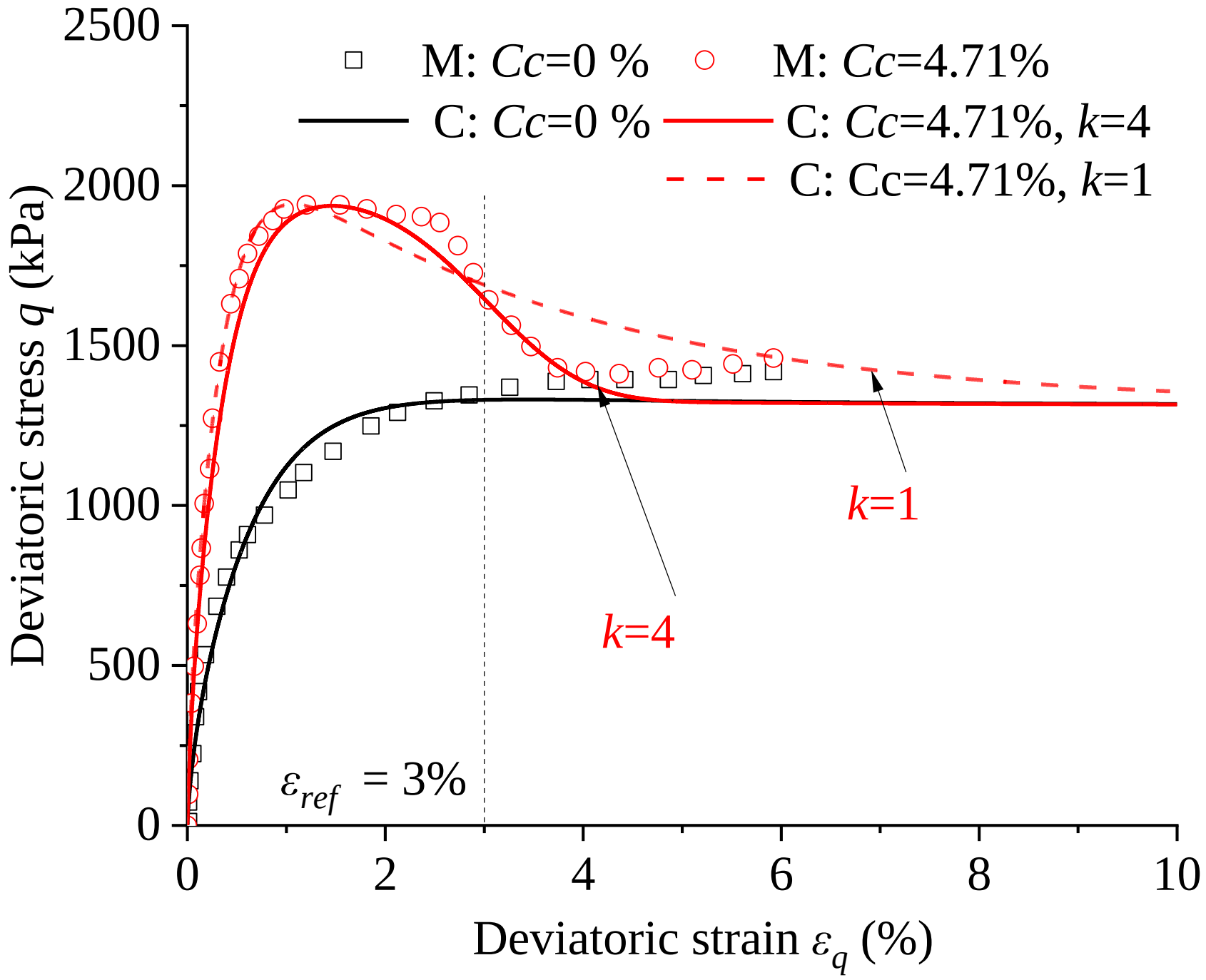

Fig. 11b

Click here to access/download;Figure;Figure 11b.pdf

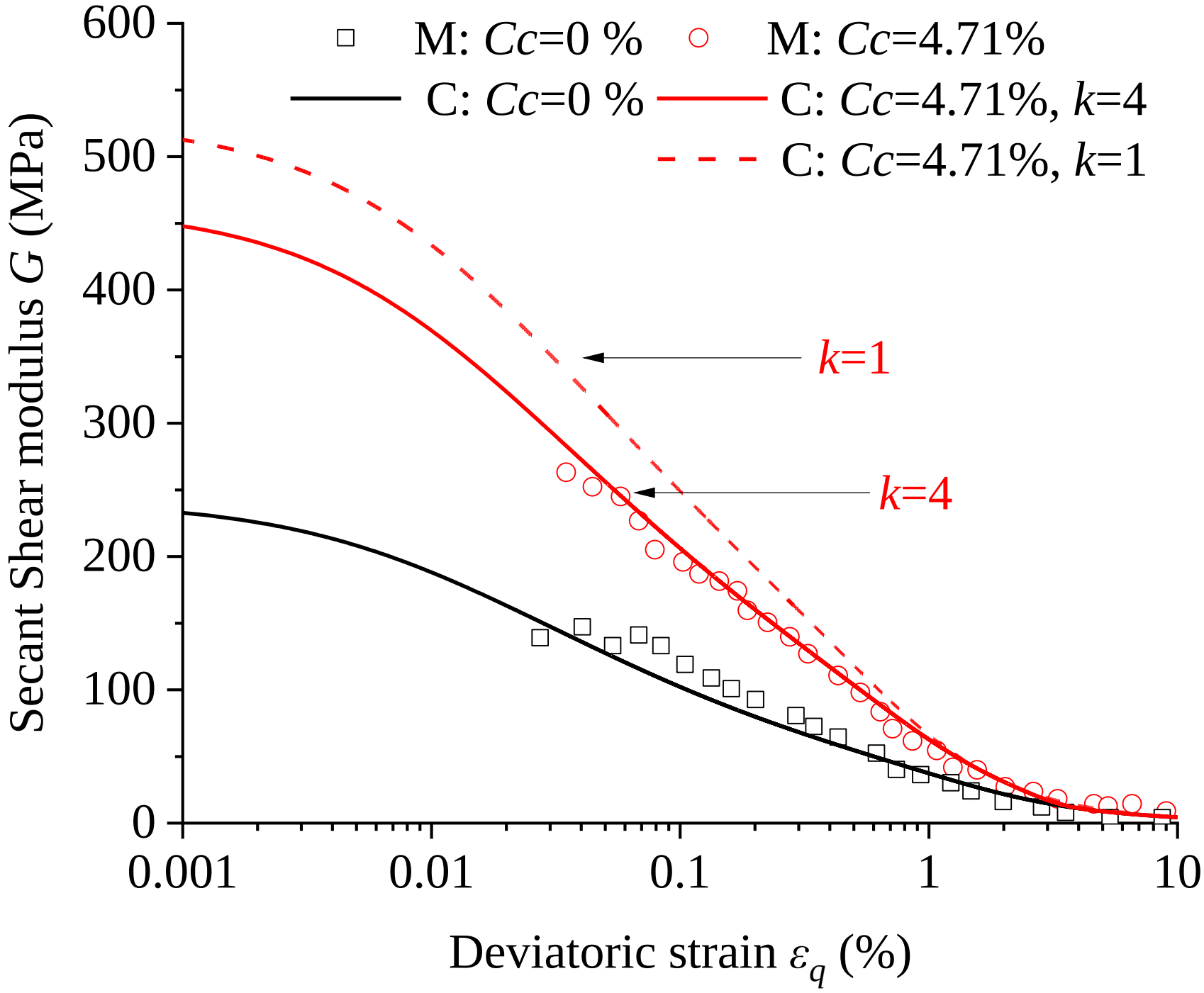

Fig. 11c

Click here to access/download;Figure;Figure 11c.pdf

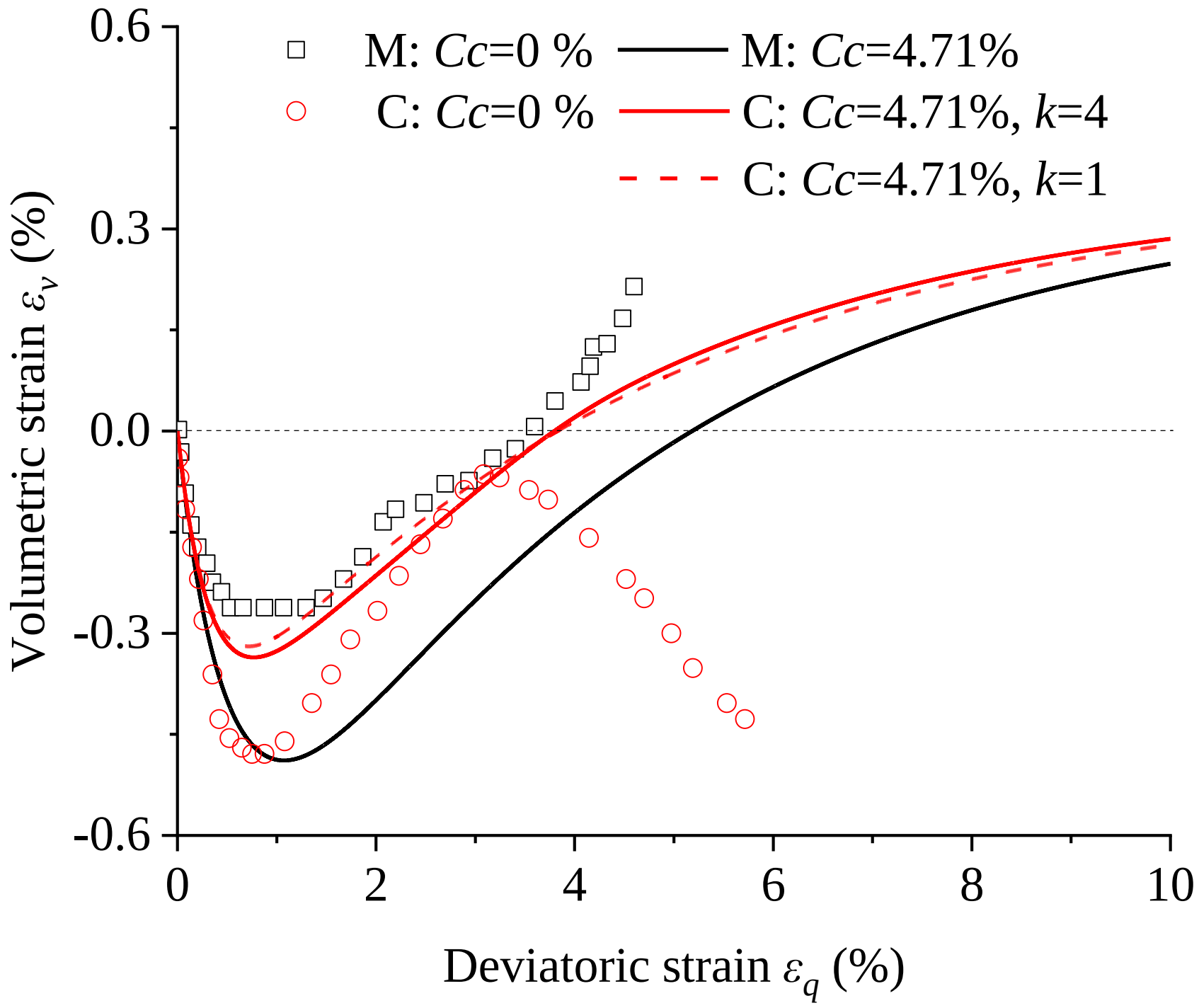

Fig. 12a

Click here to access/download;Figure;Figure 12a.pdf

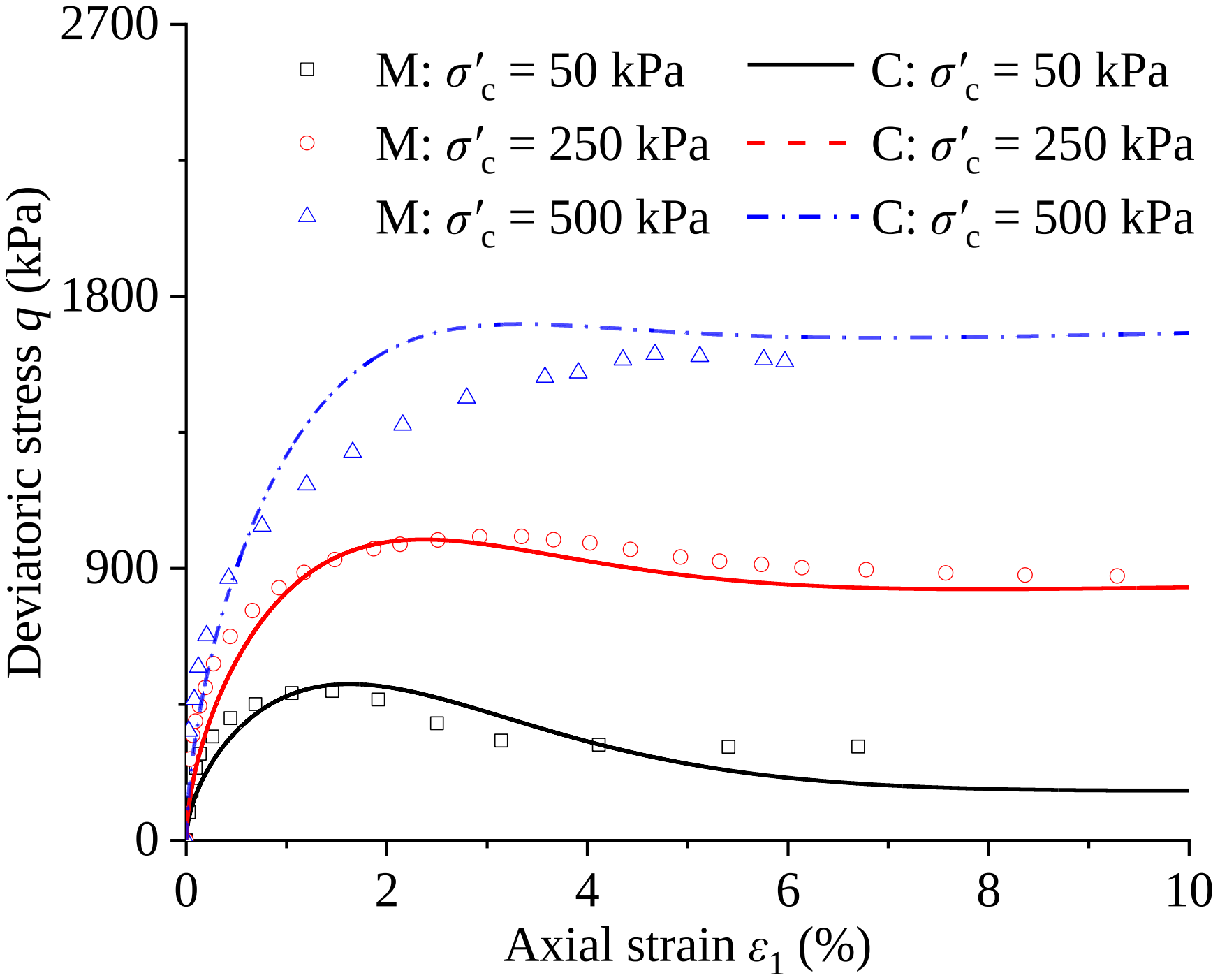

Figure 12b

Click here to access/download;Figure;Fig. 12b.pdf

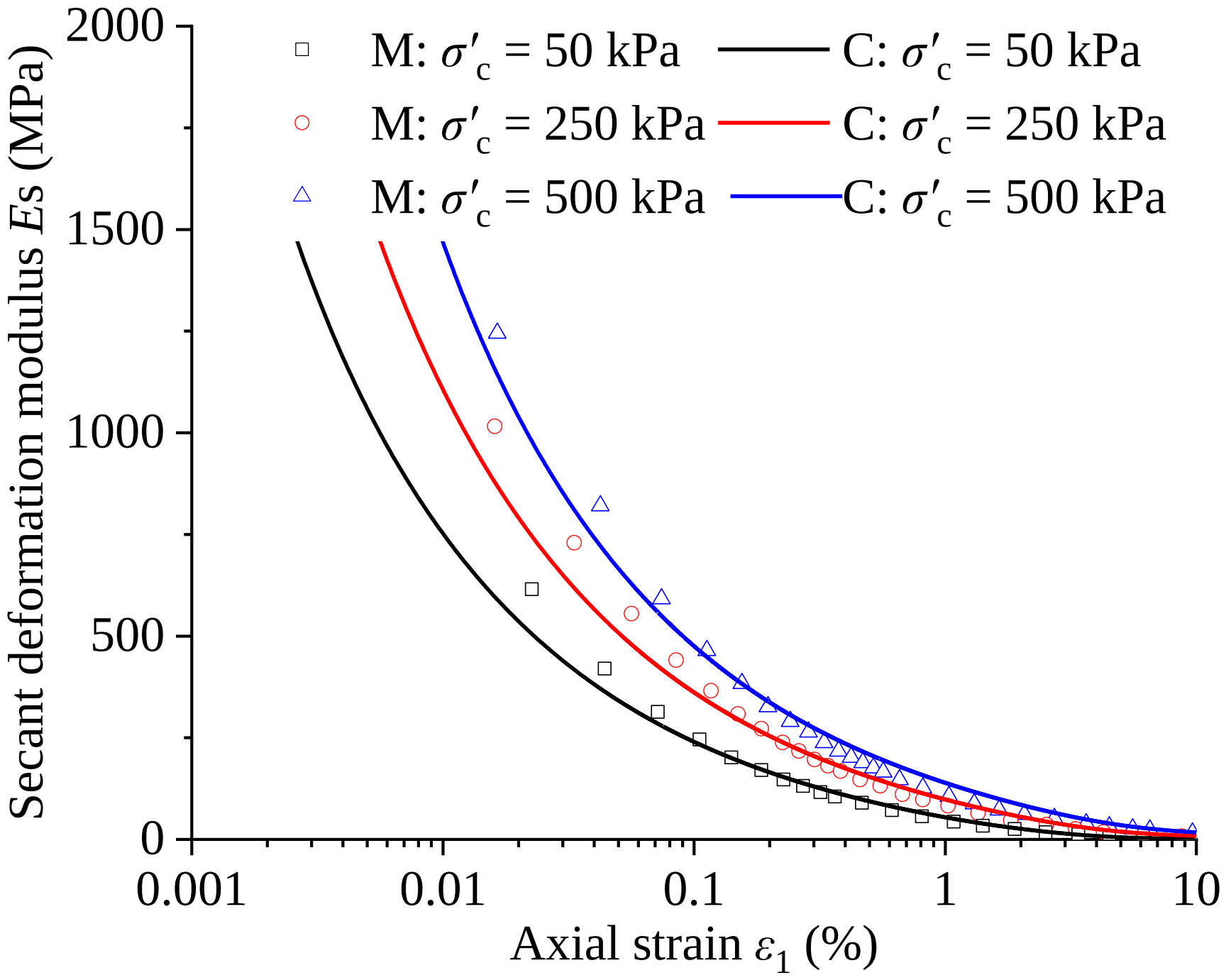

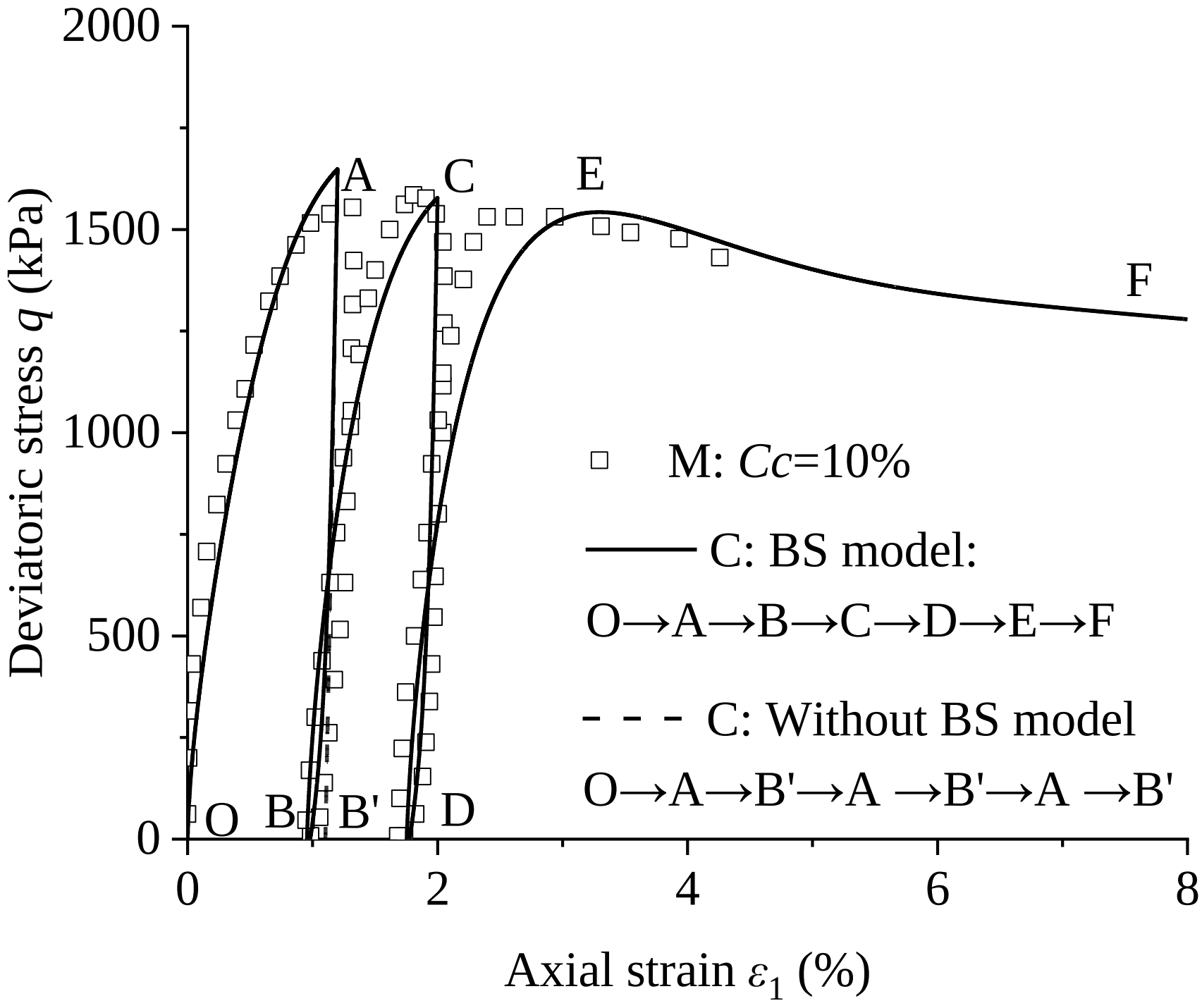

Fig. A1a

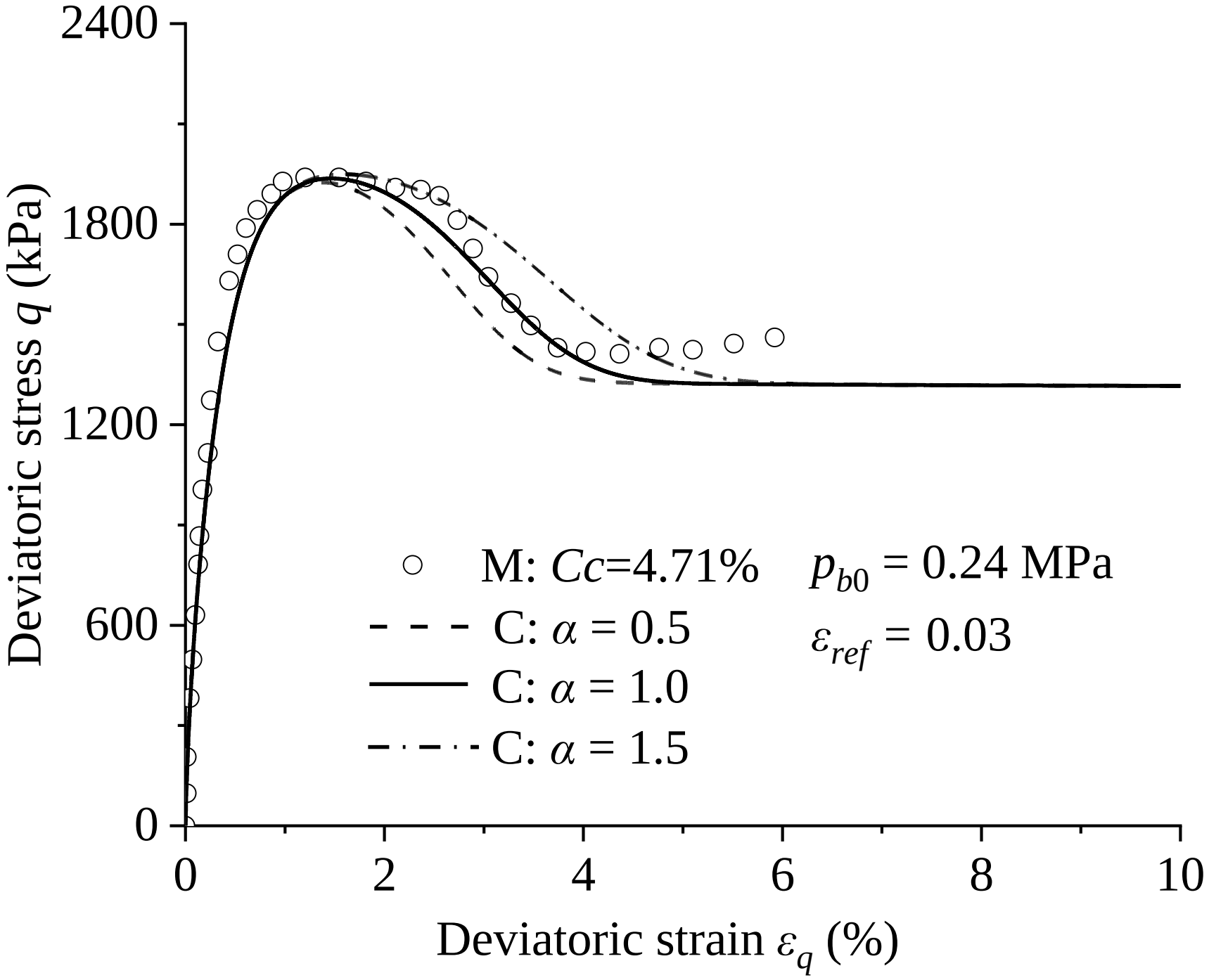

Fig. A1b

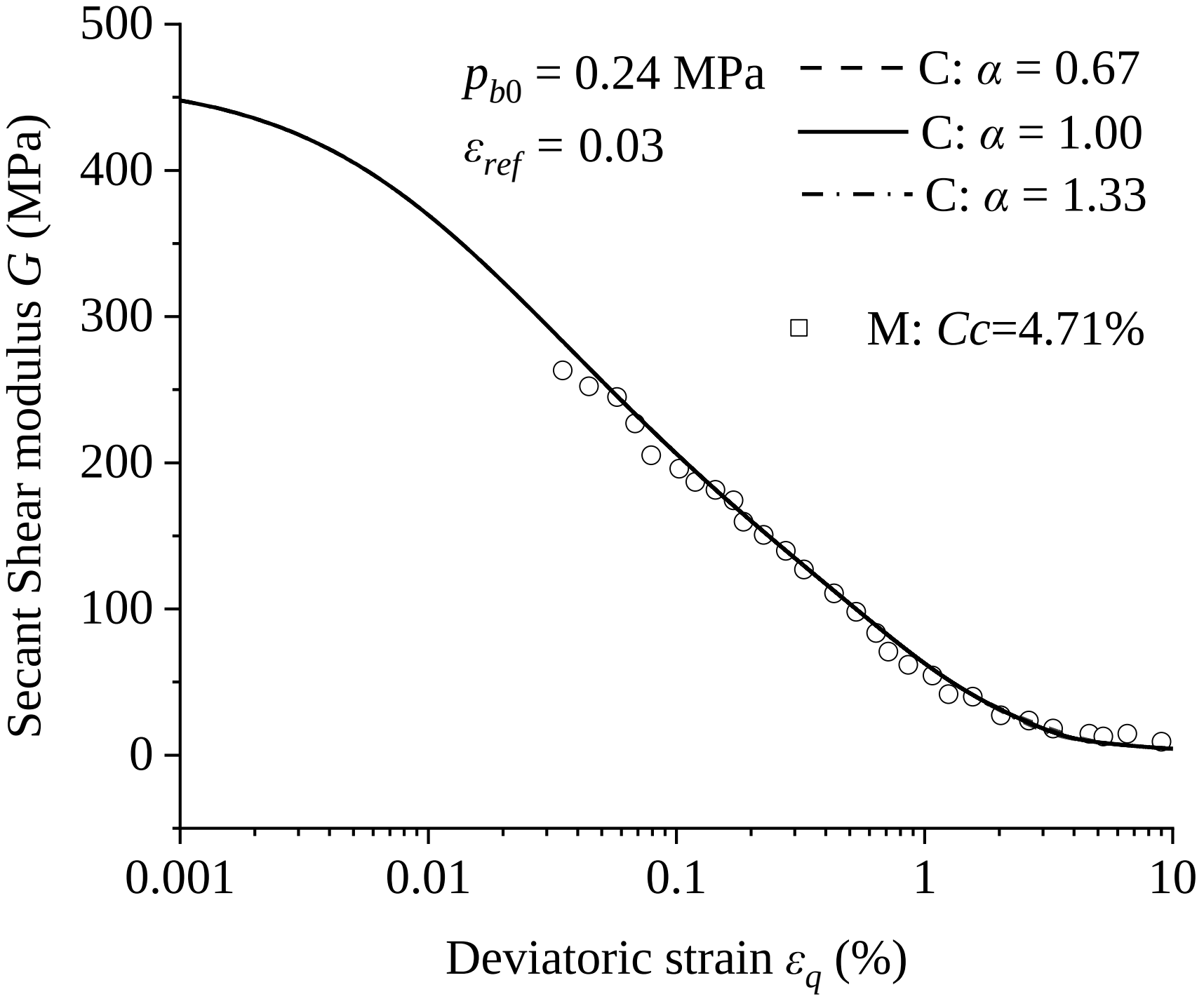

List of figures

Figure 10. Comparison between the measured (M) (Yao 2017) and computed (C) stiffness degradation curves of cemented marine clay with different cement contents: (a) *Cc* = 20%; (b) *Cc* = 30%; (c) *Cc* = 50%.

Figure 11. Comparison between the measured (M) (Marques et al. 2021) and computed (C) strength and stiffness of cemented Osorio sand: (a) stress-strain behavior; (b) degradation of stiffness. (c) volumetric strain versus shear strain.

Figure 12. Comparison between the measured (M) (Consoli et al. 2000) and computed (C) strength and stiffness of cemented weathered sandstone. (a) stress-strain behavior; (b) degradation of stiffness.

Figure 13. Comparison of calculation results between boundary surface model and classical elastoplastic model

Figure A1. Influence of parameter a on (A1.a) stress-strain behavior; (A1.b) small strain stiffness degradation.